Available online at www.sciencedirect.com
SCIENCE DIRECT®
Coordination Chemistry Reviews 238–239 (2003) 291–314
COORDINATION CHEMISTRY REVIEWS
www.elsevier.com/locate/ccr

Modeling the spin-dependent properties of open-shell Fe(III)-containing systems: towards a computational description of nitrile hydratase

Amy J. Boone [1], Christopher H. Chang [2], Shannon N. Greene, Thomas Herz [3], Nigel G.J. Richards *

Department of Chemistry, University of Florida, Box 117200, Gainesville, FL 32611-7200, USA

Received 12 June 2002; accepted 5 September 2002

Contents

Abstract

The role of metalloenzyme structure in modulating transition metal reactivity is often difficult to assess using experimental approaches. For example, the structural features of the protein that underpin the low-spin preference of the non-heme Fe(III) in

* Corresponding author. Tel.: +1-352-392-3601; fax: +1-352-392-7918.
E-mail address: richards@qtp.ufl.edu (N.G.J. Richards).
[1] Present address: Department of Biochemistry and Biophysics, University of North Carolina, Chapel Hill, NC 27599, USA.
[2] NIH Postdoctoral Fellow (DK61193).
[3] Present address: 4SC AG, Am Klopferspitz 19a, 82152 Martinsried, Germany. Supported by a postdoctoral fellowship from the Deutscher Akademischer Austauschdienst (DAAD) and the National Science Foundation (CHE-0079008).

PII: S0010-8545(02)00254-0

nitrile hydratase (NHase), and the importance of this spin-state to the catalytic mechanism, are unlikely to be determined solely by site-directed mutagenesis and/or characterization of model Fe(III) complexes. Density functional theory (DFT) calculations represent a method for determining the electronic structure of metal centers in enzymes, investigating the properties of hypothetical intermediates in the reaction mechanism, and probing the importance of specific protein residues in controlling metal chemistry. In particular, DFT methods are becoming widely used for delineating effects associated with the spin-dependent reactivity of transition metal complexes. The application of DFT calculations to the study of open-shell systems is, however, fraught with difficulties in both the technical aspects of performing such calculations and the interpretation of results. So as to illustrate these issues for the non-expert, we provide a brief overview of the theoretical basis, performance and limitations of recent DFT studies on a series of Fe(III) complexes that are models for the unusual non-heme Fe(III) center in NHase.

Keywords: Density functional theory; Nitrile hydratase; Fe(III) complexes; Spin-dependent properties; Computational bioinorganic chemistry; QM/MM calculations; Solvent effects

1. Introduction

Recent developments in density functional theory (DFT) are enabling computational studies of transition metal-containing systems containing large numbers of heavy atoms, including models of the active sites in metalloproteins [1–10]. While there are now a substantial number of examples that have calibrated the use of DFT methods in modeling reaction intermediates and transition states for closed-shell systems [11–15], much less is known about whether DFT calculations may be used to define: (i) the ground state spin preferences of open-shell transition metal complexes; (ii) spin-dependent molecular properties; and (iii) the effects of spin state on metal reactivity [16–18]. Indeed, the validity of using DFT calculations to sort spin states has been questioned because DFT is considered to model ground states rather than electronic excited states [19]. The goal of this review is to provide an overview of our recent efforts to employ DFT calculations in determining the spin-dependent energetics and structure of a series of Fe(III) complexes that are models for the unique metal center in nitrile hydratase (NHase), an enzyme that plays a key role in removing potentially toxic nitrile derivatives that are formed in plant and bacterial metabolism [20–24]. Our discussion will be divided into three main sections. First, the properties of NHase that have sparked theoretical interest in this enzyme will be described, together with a summary of Fe(III) complexes that have been prepared as models for the NHase metal center. In the second section, we will present a brief overview (for the non-expert) of the theoretical ideas underlying the concept of spin contamination, and the use and limitations of DFT methods in computing spin state-dependent properties of open-shell transition metal complexes. Finally, we will present recent results for a series of Fe(III) complexes that suggest DFT and DFT/MM calculations should provide useful insight into the electronic structure of the NHase metal center and the catalytic mechanism of the enzyme.

2. Background

2.1. Nitrile hydratase: an unusual Fe(III)-dependent enzyme

The hydration of nitriles to amides (Eq. (1)) is catalyzed by NHase [25–30], a non-heme/non-corrinoid metalloenzyme that contains either Fe(III) or Co(III) in the active site [31–33]. Bioinorganic interest in NHase

$$R-C{\equiv}N \overset{H_2O}{\underset{NHase}{\rightarrow}} R-CONH_2 \quad (1)$$

has, in part, arisen from the observation that the two forms of the enzyme are unusual in that they possess a mononuclear, low-spin ($S=1/2$) Fe(III) or ($S=0$) Co(III) center [34,35]. This ground state spin preference is not observed in other metalloenzymes possessing non-heme Fe(III) or Co(III) centers [36]. In sharp contrast to cobalt-containing NHases [35,37–39], iron-dependent NHases, such as that isolated from *Rhodococcus* sp. N-771 [27–30], exhibit a unique photoreactivity that may be used to regulate NHase activity in their host organisms. X-ray crystal structures of: (i) the native, iron-dependent NHase isolated from *Rhodococcus* sp. R312 [40]; (ii) an inactive, nitrosylated form of NHase present in *Rhodococcus* sp. N-771 [41]; and (iii) the cobalt-containing NHase from *Pseudonocardia thermophila* JCM 3095 [42] have been reported at 2.65, 1.7 and 1.8 Å resolution, respectively. All three structures show that NHase is composed of two subunits (α and β) and that the intact enzyme crystallizes as a dimeric complex (Fig. 1A). Remarkably, the primary structures of the α/β subunits present in the Fe-containing NHases are identical even though these proteins are isolated from different species. Both X-ray structures of the Fe(III)-dependent NHase show that the metal is octahedrally coordinated by two deprotonated backbone amide nitrogens (Ser-113,Cys-114) and three side chains of conserved cysteine residues (Cys-109, Cys-112, Cys-114) located only in the α subunit, and a sixth ligand. These observations were unexpected on the basis of prior resonance Raman, EXAFS and ENDOR experiments

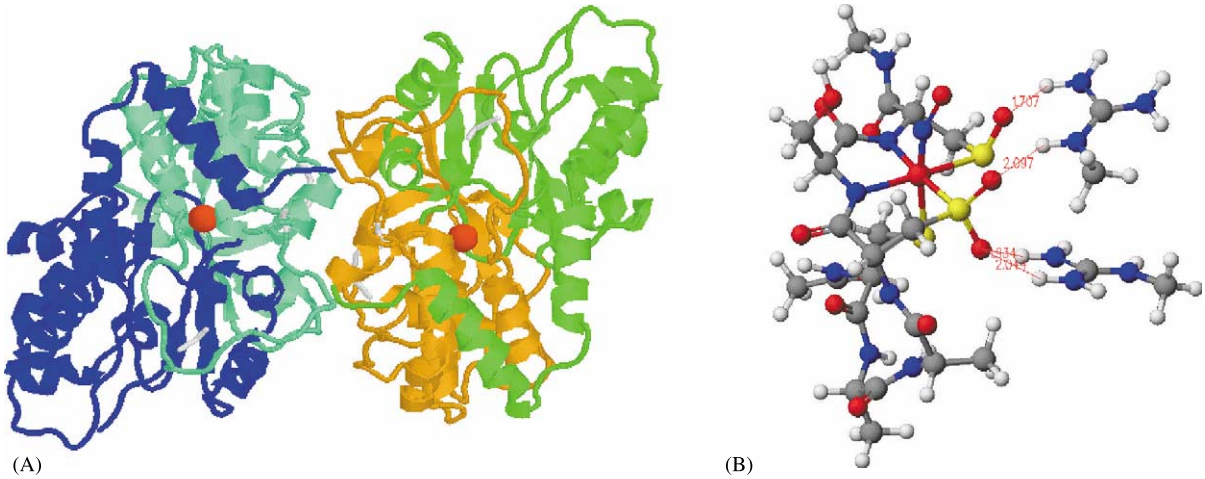

Fig. 1. (A) Cartoon representation of the crystal structure of NHase, showing the dimer composed of two independent α- and β-subunits. Protein molecules are colored in blue, cyan, yellow and orange, and the two Fe(III) centers are shown as red spheres. (B) Close-up of the Fe(III) center in the active site of NHase complexed by nitric oxide, showing the hydrogen bonding between the conserved arginine residues, Arg-56 and Arg-141, (β-subunit) and the post-translationally modified thiolate ligands of Cys-112 and Cys-114 (α-subunit). Atoms are colored using the following scheme: C, grey; H, white; N, blue; O, red; S, yellow; Fe, orange.

[31,43–45], and indeed the involvement of backbone amides as metal ligands is very unusual, the only other example being observed in the P-cluster of nitrogenase [46]. Perhaps the most intriguing finding, however, was that two of the sulfur ligands from Cys-112 and Cys-114 were post-translationally oxidized to the sulfenic (SOH) and sulfinic (SO_2H) acids, respectively, in the structure of the inactive NHase–NO complex [41] (Fig. 1B). These modifications were not observed for the Fe(III) center in the free enzyme. Independent experiments employing mass spectroscopic methods have confirmed the presence of both modifications in the NHase–NO complex [41,47], but suggest that only the sulfinic acid form of the Cys-114 side chain is present in native, active NHase [42,48]. More recent work has supported the hypothesis that oxidation of the sulfur ligands may be an essential element in NHase activation after ribosomal translation of the enzyme [41]. The non-corrin cobalt at the catalytic center of the Co(III)-dependent NHase is also coordinated by post-translationally modified cysteine residues that are identical to those observed in the complex between NO and the Fe(III)-dependent NHase [42]. Sulfur oxidation may be required for the formation of hydrogen bonds that correctly position conserved arginine residues (Arg-56, Arg-141 in the *Rhodococcus* sp. N-771 NHase) located on the β subunit within the active site [41]. Some support for the importance of these residues in the catalytic mechanism has been provided by site-directed mutagenesis experiments in which the replacement of Arg-56 gives a mutant enzyme that exhibits 1% of the NHase activity observed for the wild type enzyme [49]. The expression of recombinant NHase is not trivial, however, and so the biological significance of the sulfur oxidation remains to be definitively established. In addition to these interesting structural features and the unique spin preference of the non-heme metal center, iron-dependent NHases exhibit a characteristic, broad electronic absorption near 700 nm that has been proposed to arise from sulfur to iron charge transfer [44,50].

2.2. Inorganic Fe(III) complexes as models for NHase

The structure and unique electronic properties of the Fe(III) center are remarkably complex in light of the relatively simple reaction that is catalyzed by NHase, raising questions concerning the mechanistic importance of the unusual post-translational modifications, the role of the protein environment in modulating metal reactivity, and the catalytic intermediates underlying NHase activity. Until recently, experimental efforts to address these issues have focused on the preparation and characterization of a relatively large number of Fe(III) and Co(III) complexes that seek to mimic the active site metal coordination observed in NHases [51–63]. Many of these studies have been the subject of recent reviews [64–66]. Model complexes containing deprotonated carboxamido nitrogens and sulfinato ligands reproduce the electronic properties of the enzyme [52,67,68], and provide support for the idea that the unusual amide coordination in the enzyme serves to stabilize the metal center against reduction and reaction with dioxygen [52,67]. Octahedral complexes containing two *cis*-thiolate and imine ligands also appear to reproduce the electronic properties of NHase [56,58,59], and an interesting five-coordinate Fe(III) complex has been synthe-

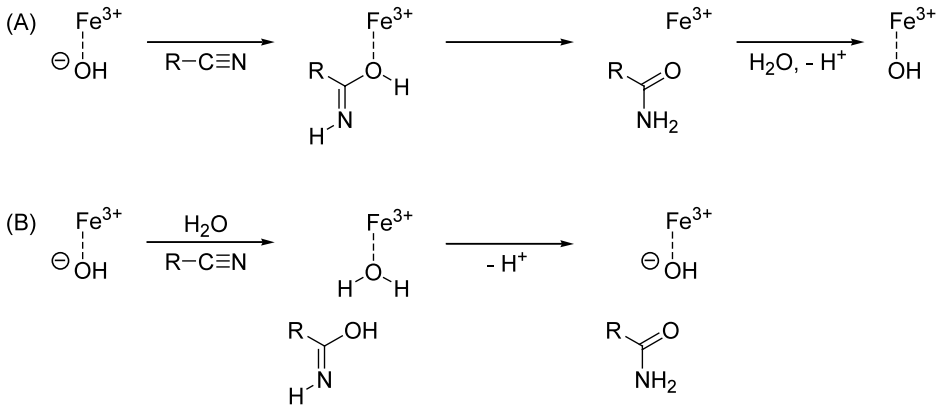

Scheme 1. Proposed mechanistic roles for a metal-bound hydroxide in NHase-catalyzed nitrile hydration. (A) The metal-bound hydroxide acts as a nucleophile and reacts with the bound nitrile to give a metal-bound intermediate that is released to give a coordinately unsaturated Fe(III) species to which water can bind. (B) The metal-bound hydroxide acts as a base to activate an active site water for nucleophilic attack upon the nitrile. This gives a tautomer of the product amide and a metal-bound water that can lose a proton to regenerate the active form of the enzyme.

sized that can bind either NO [58] or azide [59] (a competitive inhibitor of NHase) to form a six-coordinate complex with spectral properties similar to the those of the enzyme. Although definitive conclusions cannot be made in the absence of kinetic experiments on NHase itself, it has been shown that the sulfur coordination modulates the acidity of metal-bound water, and suggests that metal-bound hydroxide could be responsible for the hydration of nitriles at the active site (Scheme 1) [69]. None of the model Fe(III) complexes synthesized to date has exhibited the ability to catalyze nitrile hydration, however, and only one functional Co(III) model complex has been prepared that can convert acetonitrile to acetamide at high pH. Moreover, attempts to oxidize thiolate ligands in Fe(III) complexes have, with only a single exception [70], yielded sulfinato derivatives in which oxygen rather than sulfur is bound to the metal [62]. In contrast, oxidation of a model Co(III) complex with hydrogen peroxide at low temperature did give sulfinato derivatives in which the metal remained coordinated by sulfur [53].

Although the characterization of inorganic model Fe(III) and Co(III) complexes has provided valuable insights into the reactivity and spectroscopy of the non-heme Fe(III) site in NHase, they cannot provide information on the role of the protein environment in modulating the electronic and chemical properties of the metal. In addition, no model complex has yet been prepared with a reversibly photolabile Fe(III)–NO bond, although the characterization of candidate complexes is a subject of active investigation [51]. With the availability of high-resolution structural information on the enzyme and on a significant number of good model Fe(III) complexes, however, theoretical calculations of electronic structure and reactivity [71] represent a complementary approach for investigating the roles of the unusual metal coordination and protein environment in giving rise to the unique spin and spectroscopic properties of the Fe(III) center in NHase.

Calculating the properties of transition metal-containing systems is a significant challenge for ab initio quantum mechanical (QM) methods [10], particularly those involving first-row elements such as iron, which possess a manifold of electronic states with different chemical behavior lying close in energy [71–73]. The need to include dynamic and static electron correlation demands the use of high-level QM techniques, such as MCSCF [74,75] and CASPT2 [76–78] that require significant computational effort, often limiting the size of transition metal complexes to those containing only a few heavy atoms in addition to the metal. Correctly modeling dynamical correlation also exacerbates the difficulty of these calculations because large basis sets must be used [79]. Although semi-empirical methods are a relatively inexpensive approach to modeling the electronic structure of large molecules [80,81], the development of parameters to compute the structures of molecules containing metals with unfilled d orbitals has proven a difficult problem [82]. DFT calculations therefore represent the only practical method for computing the structural properties of transition metal complexes [83–86] and metalloenzyme active sites [1–10,87–92]. There are, however, a number of traps for the unwary computational chemist in employing DFT methods to study the electronic structure and molecular properties of open-shell systems [10], such as those containing Fe(III) [93]. These problems include: (i) difficulties in obtaining converged wavefunctions; and (ii) artifacts introduced into the calculations by spin contamination [94]. We will therefore briefly describe the theoretical basis of these issues prior to describing the results of our recent DFT studies upon the spin state energetics, and spin state-dependent structures, of NHase model Fe(III) systems.

3. Spin states and spin contamination in molecular orbital (MO) theory

3.1. Hartree–Fock (HF) MO treatment of open-shell systems

To understand the issues in employing DFT methods to compute the spin state-specific properties of Fe(III) complexes, several important concepts are best introduced using a MO-based description of polyatomic molecules [94,95]. As usual, we assume the Born–Oppenheimer approximation in which the nuclei are regarded as having fixed positions. Since Fe(III)-containing molecules are open-shell systems, we will limit our discussion to unrestricted HF calculations, in which the N-electron molecular wavefunction is approximated as a set of N one-electron 'spin orbitals', χ_i, each comprising a product of both a one-electron spatial orbital, φ, and a spin function. The determinant describing the ground state, unrestricted $\Psi^{(0)}$ of a molecule may be written in the following general form:

$$\Psi^{(0)} = |\varphi_1\bar{\varphi}_2\varphi_3\bar{\varphi}_4 \ \cdots \ \varphi_{(n-1)}\bar{\varphi}_n|$$

Here the spatial orbital functions are denoted by φ, and the bar denotes a beta (β) spin function, as opposed to an alpha (α) spin function.

The spin orbitals χ_i are eigenfunctions of the Fock operator $f^\sigma(1)$, and their energies are given by the eigenvalues ε_i of the following equation:

$$f^\alpha(1)\chi_a^\sigma(1) = \varepsilon_a^\sigma\chi_a^\sigma(1)$$

For a molecule containing N^α α-spin electrons and N^β β-spin electrons (with $N^\alpha \geq N^\beta$ by convention), the HF approach converts the N-electron problem to two sets of one-electron problems. Thus, separate Fock operators are written for electrons of spin α and β that have the following form:

$$f^\alpha(1) = h(1) + \sum_a^{N^\alpha}[J_a^\alpha(1) - K_a^\alpha(1)] + \sum_a^{N^\beta} J_a^\beta(1)$$

$$f^\beta(1) = h(1) + \sum_a^{N^\beta}[J_a^\beta(1) - K_a^\beta(1)] + \sum_a^{N^\alpha} J_a^\alpha(1)$$

In these equations, the first term represents the kinetic energy of the electron and its potential energy arising from its interaction with the fixed nuclei in the molecule. The interactions of this electron with the other $N-1$ electrons in the molecule are described by the second and third terms, which contain $J_a^\sigma(1)$ and $K_a^\sigma(1)$. The last summation in each equation adds in Coulomb repulsion between electrons of different spins. Note that these separate equations prevent the exchange of α- and β-spin electrons, although the presence of α- and β-spin operators in the equations for $f^\alpha(1)$ and $f^\beta(1)$, respectively, demonstrates that the two sets of equations are coupled and so must be solved together.

The expression for the total electronic energy of a molecular system when computed using an unrestricted HF description is then given by [94]:

$$E_0 = \sum_a^{N_\alpha} h_{aa}^\alpha + \sum_a^{N_\beta} h_{aa}^\beta + \frac{1}{2}\sum_a^{N_\alpha}\sum_b^{N_\alpha}(J_{ab}^{\alpha\alpha} - K_{ab}^{\alpha\alpha}) + \frac{1}{2}\sum_a^{N_\beta}\sum_b^{N_\beta}(J_{ab}^{\beta\beta} - K_{ab}^{\beta\beta}) + \sum_a^{N_\alpha}\sum_b^{N_\beta} J_{ab}^{\alpha\beta}$$

where:

$$h_{aa}^\sigma = \int_0^\infty \mathrm{d}\vec{r}_1 \ \chi_a^\sigma(1)\left(-\frac{1}{2}\nabla_1^2 - \sum_A \frac{Z_A}{|\vec{r}_1 - \vec{R}_A|}\right)\chi_a^\sigma(1)$$

in which ∇^2 is the kinetic energy operator, and Z_A and $\vec{R}_A$ are the charge and coordinates of the Ath nucleus, respectively. The integrals J_{ab} and K_{ab} take the following forms:

$$J_{ab} = \int_0^\infty\int_0^\infty \mathrm{d}\vec{r}_1 \ \mathrm{d}\vec{r}_2 \ \chi_a^*(1)\chi_b^*(2)\frac{1}{r_{12}}\chi_a(1)\chi_b(2) \quad \text{and}$$

$$K_{ab} = \int_0^\infty\int_0^\infty \mathrm{d}\vec{r}_1 \ \mathrm{d}\vec{r}_2 \ \chi_a^*(1)\chi_b^*(2)\frac{1}{r_{12}}\chi_a(2)\chi_b(1).$$

The first of these integrals, J_{ab}, arises from the orbital-averaged Coulombic repulsion of two electrons of like spin. The meaning of the exchange integral, K_{ab}, is less intuitive in that its essential physical interpretation is the exchange of two electrons between two orbitals of like spin (but not between orbitals of opposite spin) in the molecule, a process that lowers the energy. An important feature of the HF approach is that these integrals must be evaluated for spin orbitals χ_a and χ_b that may have no significant interaction or are spatially separated within the structure, i.e. non-local interactions must be computed. Using iterative procedures, the HF equations can be solved numerically to yield descriptions of the MOs and their associated energies [96]. For open-shell molecular systems, such as those containing Fe(III), the HF exchange stabilization energy is proportional to the number of excess electrons, and, as a consequence, ground state configurations for molecules containing a higher number of unpaired electrons tend to be lowest in energy in unrestricted HF calculations.

3.2. Spin contamination in UHF calculations

A given spin projection of a molecular system is defined by the number of unpaired electrons, i.e. the difference between N^α and N^β, where these are numbers of electrons having α and β spins, respectively. A

wavefunction associated with a pure molecular spin state is an eigenfunction of both the spin operators $\hat{S}^2$ and $\hat{S}_z$. For example, a physical quartet spin state is defined by the quantum number $S = 3/2$ [97], for which the possible S_z spin projections ($S_z = \pm 3/2$ and $\pm 1/2$) give rise to a multiplicity of 4. The multiplicity that is initially specified in an unrestricted HF calculation determines the orbital occupation, i.e. the number of electrons of spin α and β, which correspond to the eigenvalue S_z. For any pure spin state, the expectation value of the $\hat{S}^2$ operator ($\langle \hat{S}^2 \rangle_{\text{exact}}$) is given by:

$$\langle \hat{S}^2 \rangle_{\text{exact}} = \left(\frac{N^\alpha - N^\beta}{2} \right) \left(\frac{N^\alpha - N^\beta}{2} + 1 \right)$$

The exact expectation value of $\hat{S}^2$ for a spin eigenfunction with three excess α-spin electrons ($N^\alpha - N^\beta = 3$) is therefore $3/2 \cdot 5/2 = 15/4$. Although the wavefunctions obtained from UHF calculations are eigenfunctions of the $\hat{S}_z$ operator (defined by the net sum of the projections of the excess α-spin electrons), they are not eigenfunctions of $\hat{S}^2$ (which is related to α/β orbital overlap), leading to the concept of 'spin contamination'. For example, the UHF wavefunction obtained for a

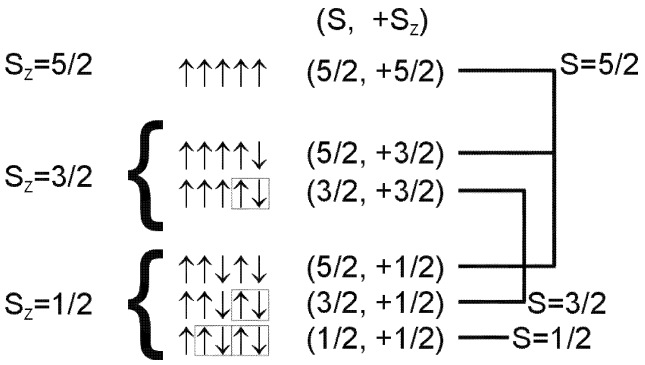

Fig. 2. In spin-unrestricted calculations, the minimum energy set of MOs corresponds to a linear combination of spin microstates of specified S_z over the possible spin states S. The magnitude of the spin angular momentum, S, is the experimentally observed spin state. In studies of the sextet state ($S = 5/2$) of Fe(III), unrestricted calculations should represent an essentially pure spin microstate (S, S_z) = (5/2, 5/2) from within a spin manifold because there can be no contamination from S_z components of a lower spin state. This is the case since the only possible values of S_z for lower spin states are all less than 5/2. Hence, the calculated $\langle \hat{S}^2 \rangle$ value will be close to the expected value of $2S+1 = 6$. On the other hand, problems may arise when lower multiplicities are input for a given Fe(III) complex. For example, if a 'doublet spin multiplicity' is specified for Fe(III), then three contributing spin microstates (S, S_z) = (1/2, 1/2), (3/2, 1/2) and (5/2, 1/2) may be mixed into the wavefunction that is obtained from the calculation, i.e. the molecular wavefunction is actually a combination of the spin microstates, each of which in turn is described by one or more Slater determinants. The amount of spin contamination will vary depending on how closely opposite spins are paired in the valence level. Large deviations from $\langle \hat{S}^2 \rangle_{\text{exact}}$ are a strong indicator that the set of MOs and the calculated energy are not accurate. In the figure, boxes denote 'perfectly paired' α- and β-spin electrons, and unboxed arrows denote electrons in orthogonal spin-orbitals.

doublet spin projection of Fe(III) ($N^\alpha - N^\beta = 1$) might be contaminated with those associated with quartet and sextet spin-states, i.e. the wavefunction is a mixture of functions with (S, S_z) = (1/2, 1/2), (3/2, 1/2) and (5/2, 1/2) (Fig. 2). This spin-contaminated UHF wavefunction yields a computed total energy lower than, or equal to, that obtained for the case where every β-spin is constrained to be perfectly paired with an α-spin (corresponding to a special case of the 'restricted open-shell' quantum chemical description when all unpaired spins are parallel, which does give wavefunctions that are eigenfunctions of both $\hat{S}^2$ and $\hat{S}_z$), because the greater variational freedom within the unrestricted approximation gives a more accurate representation of the true wavefunction. Clearly, directly comparing spin-contaminated UHF solutions of varying S as approximations to spin states presents difficulties in quantitative interpretation. Furthermore, high levels of spin contamination will lead to errors in the computed molecular geometries, population analyses and spin densities for a system of a given spin angular momentum, S.

The basis of spin contamination in MO-based ab initio calculations is perhaps most easily understood [98] by writing the expectation value of the $\hat{S}^2$ operator as:

$$\langle \hat{S}^2 \rangle_{\text{UHF}} = \langle \hat{S}^2 \rangle_{\text{exact}} + N^\beta - \sum_i^{N_\alpha} \sum_j^{N_\beta} |W_{ij}^{\alpha\beta}|^2$$

where $W_{ij}^{\alpha\beta}$ is the overlap integral of the spatial orbitals containing the α and β electrons, and N^α and N^β correspond to the number of α and β electrons, respectively, such that $N^\alpha \geq N^\beta$ and $N^\alpha + N^\beta = N$, the total number of electrons. If, aside from the excess α-electrons, there is perfect overlap between α- and β-spatial orbitals (perfect pairing); the last term will simply evaluate to N^β, and $\langle \hat{S}^2 \rangle_{\text{UHF}}$ will take its exact value. However, if the last two terms of this expression do not cancel, then $\langle \hat{S}^2 \rangle_{\text{UHF}}$ will be greater than $\langle \hat{S}^2 \rangle_{\text{exact}}$ and the wavefunction will be spin-contaminated. Although restricted open-shell Hartree–Fock (ROHF) calculations can overcome this problem by forcing the last term to equal N_β, the necessary constraints that must be used decrease the variational freedom and generally result in an increase in the calculated energy of the system.

As a check for the presence of spin contamination in UHF calculations, most programs compute the expectation value of the total spin, $\langle \hat{S}^2 \rangle_{\text{UHF}}$. In the case of calculations on organic compounds, spin contamination is often considered to be negligible if the values of $\langle \hat{S}^2 \rangle_{\text{UHF}}$ and $\langle \hat{S}^2 \rangle_{\text{exact}}$ differ by less than 10%. A similar empirical rule for transition metal complexes, however, remains to be established. An alternate expression for characterizing the extent of spin contamination is given by [99]:

$$2S+1=\sqrt{4\langle\hat{S}^2\rangle_{\mathrm{UHF}}+1}$$

In this equation, S is the total spin angular momentum of the unpaired electrons. Deviations from integer values of $(2S+1)$ provide a useful measure of the level to which the UHF wavefunction is spin-contaminated.

Despite the problems outlined above, the UHF approach is a popular method for treating the energetics of organic radicals and other open-shell systems, which has stimulated the development of strategies for removing spin contamination. These can be best understood by considering an approximate method that has been used to obtain properties associated with systems that are open-shell singlets [100]. In this case, the UHF single determinant is a mixture of the singlet and triplet states, and is given by the following expression:

$$|\phi_1\alpha(1)\phi_2\beta(2)|\pm|\phi_1\beta(1)\phi_2\alpha(2)|$$

Here the minus and plus combinations correspond to the singlet and triplet, respectively. If it is assumed that: (i) the energy for the triplet state, E_{T}, can be computed; (ii) the triplet state is pure and is not contaminated by contributions from higher-order spin-states; and (iii) only the triplet contaminates the open-shell singlet, then the UHF wavefunction and energy for the contaminated singlet can be written as a linear combination of a singlet and a triplet state, as shown below:

$$\Psi_{\mathrm{UHF}}=c_{\mathrm{S}}\psi_{\mathrm{S}}+c_{\mathrm{T}}\psi_{\mathrm{T}}$$

$$E_{\mathrm{UHF}}=c_{\mathrm{S}}^2E_{\mathrm{S}}+c_{\mathrm{T}}^2E_{\mathrm{T}}$$

$$c_{\mathrm{S}}^2+c_{\mathrm{T}}^2=1$$

From the first equation, it is clear that the expectation value $\langle\hat{S}^2\rangle_{\mathrm{UHF}}$ can be written as:

$$\langle\hat{S}^2\rangle_{\mathrm{UHF}}=c_{\mathrm{S}}^2\langle\hat{S}^2\rangle_{\mathrm{S}}+c_{\mathrm{T}}^2\langle\hat{S}^2\rangle_{\mathrm{T}}$$

where the other expectation values are for the pure singlet and triplet states. Using these equations, the energy of the pure singlet state, E_{S}, can be computed from the calculated singlet energy, E_{UHF}, the expectation value $\langle\hat{S}^2\rangle_{\mathrm{UHF}}$ and the triplet state energy, E_{T}, using the equation:

$$E_{\mathrm{S}}=\frac{2E_{\mathrm{UHF}}-\langle\hat{S}^2\rangle_{\mathrm{UHF}}E_{\mathrm{T}}}{2-\langle\hat{S}^2\rangle_{\mathrm{UHF}}}$$

The extension of this approach to molecular systems capable of adopting greater than two spin states cannot, however, be accomplished unless it is assumed that any given spin state is only contaminated by one other spin state.

A more general strategy for obtaining spin-specific molecular properties is to employ projection methods. For example, in projected unrestricted Hartree–Fock (PUHF) calculations [101–106], the UHF wavefunction is assumed to be a linear combination of those associated with pure spin states:

$$\Psi_{S_z}^{\mathrm{UHF}}=\sum_{S=S_z}^{S_z+N_\beta}\omega_{\mathrm{s}}\sum_{k=0}^{N_\beta}C_k(S,\ S_z)^{2S+1}\Psi_{S_z}^{k}$$

In this equation, when written in atomic units, S is the total spin angular momentum, $S_z=1/2(N^\beta-N^\alpha)$, and the squares of the weighting coefficients, ω_{s}, sum to unity for a normalized UHF wavefunction. The energy of the UHF wavefunction then takes the following form:

$$E(\Psi_{S_z}^{\mathrm{UHF}})=\sum_{k=0}^{N_\beta}\omega_{S_z+k}^2E(^{2(S_z+k)+1}\Psi_{S_z})\le E(^{2S_z+1}\Psi_{S_z}^{\mathrm{RHF}})$$

A projection operator, $\hat{O}_S$, that removes all spin components greater than the sth component can be defined as a product of annihilation operators, according to the following equation:

$$\hat{O}_S=\prod_{k\neq s}\frac{\hat{S}^2-k(k+1)}{s(s+1)-k(k+1)}$$

Applying this operator to the expanded UHF wavefunction then results in the wavefunction associated with a pure spin-state wavefunction, from which the desired molecular properties can be calculated. In general, this projection approach yields spin-state energies that are considerably lower than those obtained using standard ROHF methods, because different orbitals are allowed for the different electron spins.

3.3. Spin polarization and its complicating effect in UHF calculations

Another complicating issue that arises when carrying out spin-unrestricted calculations is that of spin polarization, i.e. when 'paired' electrons of opposite spin (α and β) have different spatial distributions within the molecule. 'Paired' and 'unpaired' electrons can be defined in terms of the overlap integral $W_{ij}^{\alpha\beta}$ for the spatial MOs containing each electron. Thus, when the α and β electrons occupy identical ($W_{ij}^{\alpha\beta}=1$) or orthogonal ($W_{ij}^{\alpha\beta}=0$) spatial orbitals, they are said to be 'paired' and 'unpaired', respectively. These ideas provide a simple conceptual model for understanding why microstates of equal S_z can be associated with different spin magnitudes, S. For example, a molecule containing equal numbers of α and β electrons may have its two highest-energy electrons paired ($S=0$, $S_z=0$) or unpaired ($S=1$, $S_z=0$). The latter arrangement is actually part of a triplet state, because it is of identical energy (in the absence of a magnetic field and spin–orbit coupling) to states containing two α electrons ($S=1$, $S_z=1$) or two β electrons ($S=1$, $S_z=-1$) since they occupy fully orthogonal orbitals ($W_{ij}^{\alpha\beta}=0$). On the other hand, when the α and β electrons are paired, then there can only be a single state due to the Pauli exclusion principle. There are an infinite number of possible spin-polarized condi-

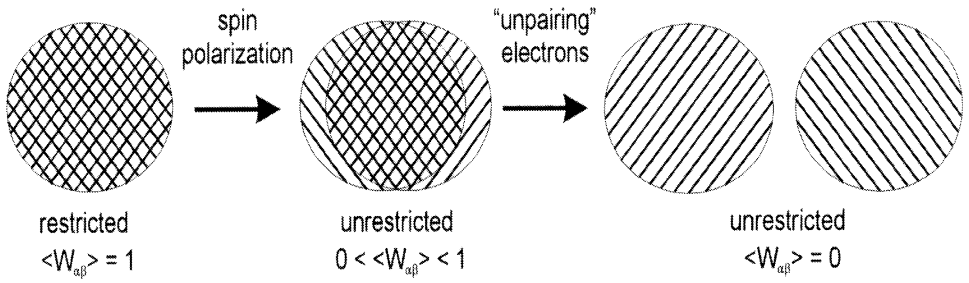

Fig. 3. In a restricted calculation, requiring every β-spin orbital to have a spatially identical α-spin orbital corresponds to 'perfect pairing' of all of the spins except the excess α-spins. Spin polarization can therefore only be described by unrestricted formalisms, in which each spin orbital has its own spatial function, and can be thought of as an intermediate state on the way to fully unpaired electrons, which have $W_{ij}^{\alpha\beta} = 0$, where $W_{ij}^{\alpha\beta}$ is the overlap integral of the α- and β-spin orbitals.

tions, however, in which the spatial orbitals containing the α and β electrons differ ($0 < W_{ij}^{\alpha\beta} < 1$), and the binary concept of 'paired' and 'unpaired' electrons becomes inappropriate (Fig. 3). So, even if there are no excess α-spin electrons ($S_z = 0$) in the molecule, the spin magnitude and thus spin state can have a finite value, which arises from α and β electrons occupying spatially orthogonal orbitals in UHF calculations. In general, while such spatial separation does not affect the net number of excess α electrons, spin polarization (as it is defined above) will always cause $\langle \hat{S}^2 \rangle$ to assume a higher value than expected. Spin polarization has been used to explain the nature of isotropic (Fermi contact) hyperfine coupling of electrons in p or d orbitals, which have no density at the nucleus [107,108].

The existence of spin polarization contributions raises questions concerning the physical interpretation of the $\langle \hat{S}^2 \rangle$ values obtained for the molecular wavefunctions computed in UHF calculations. For example, does a spin-polarized, open-shell system containing one excess α electron in the valence shell, for which $\langle \hat{S}^2 \rangle$ is computed to be greater than 0.75, really have higher spin states contaminating its ground state wavefunction? If spin polarization exists in a pure spin eigenstate, it will lead to small deviations from $\langle W_{\alpha\beta} \rangle = 1$, whereas higher spin states will correspond to one or more electron pairs becoming unpaired, thereby eliminating the contribution of one or more $\langle W_{\alpha\beta} \rangle$'s from the $\langle \hat{S}^2 \rangle_{\mathrm{UHF}}$ equation. Significant contributions from higher spin states will thus have larger effects on the magnitude of $\langle \hat{S}^2 \rangle_{\mathrm{UHF}}$. We suggest that $\langle \hat{S}^2 \rangle$ reflects a combination of effects, and therefore that large deviations from the theoretical value indicate either that a multi-determinantal approach is necessary to describe the ground state accurately, or that the 'low spin state' being calculated is actually a low S_z component of a higher spin state. Equally, small deviations in the calculated $\langle \hat{S}^2 \rangle$ value suggest that a single-determinant wavefunction provides a decent description of the molecular system in the expected spin state, and can therefore be used to determine accurate chemical properties.

In summary, the simplicity of UHF theory means that this approach has been widely employed in computing the electronic properties of open-shell systems despite the serious approximations that are present in the underlying model. For example, the HF exchange term, which is negative in sign, is proportional to the number of unpaired electrons. As a result, open-shell transition metal wavefunctions with higher spin projections tend to be energetically stabilized relative to those with lower ones, biasing the ground state spin preferences to high spin states. Spin polarization can arise from the fact that α-spin electrons only exchange with other α-spin electrons, and although the UHF method avoids the neglect of spin polarization, the effect may be artificially enhanced from using a single-determinant to describe an inherently multi-determinantal problem. The resulting spin contamination may be removed by the application of projection methods, but large errors may be observed in UHF calculations, particularly in those seeking to evaluate reaction mechanisms and activation energies.

3.4. Introducing the effects of electron correlation in MO-based methods

Electron correlation, the energy of which is formally defined as the difference between the exact energy of a system and the best possible HF estimate [94], is neglected in the HF approach. Correlation may be classified as either static or dynamic in nature. Static correlation, which arises from the need for multiple reference determinants to describe a system, may be incorporated into a wavefunction by using multi-reference methods such as multi-configurational self-consistent-field (MC-SCF) [74,75], generalized valence bond (GVB), and complete active space-self-consistent field (CASSCF) [76,95]. Dynamic correlation is attributed to the correlation of electronic motion, which prevents electrons from 'bumping into' one another and is a consequence of short-range Coulombic repulsion. Close analysis of the Coulomb operator in the UHF method reveals that only the average electron–electron repulsion

is calculated, resulting in an overestimate of electron–electron repulsion energy. Thus, if correlation were 'turned on' in a HF wavefunction, the decrease in electronic repulsion would lead to expansion of the orbitals until a new balance between electron–nuclear attraction and electron–electron repulsion were achieved. Dynamic correlation usually comprises the largest contribution to the correlation energy. A common method for incorporating correlation into HF calculations is to construct a modified wavefunction using the unoccupied 'virtual' orbitals of the 'reference' HF wavefunction. In this approach, which is termed configuration interaction (CI), contributions from excited configurations, in which electrons are promoted from the 'filled' to the 'virtual' MOs, are mixed variationally with the ground state wavefunction to give the following expression:

$$\Psi_{\mathrm{CI}} = \Phi_0 + \sum_{i,a} C_i^a \Phi_i^a + \sum_{i<j,\ a<b} C_{ij}^{ab} \Phi_{ij}^{ab} + \cdots$$

where Φ_0 is the wavefunction for the reference state, and the remaining terms include the excitation of up to N electrons from the occupied orbitals $i, j, \ldots$ to the virtual orbitals $a, b, \ldots$, where N can take the values 1, 2, 3, …, n, where n is the total number of electrons in the molecule. A fully correlated CI wavefunction would therefore be constructed from all possible configurations, and would account for all of the correlation energy, assuming an infinite basis or within a given atomic orbital basis (see below). Computing the full CI for open-shell transition metal complexes is not, however, feasible because several configurations are possible for each level of excitation due to of the large number of occupied and virtual MOs orbitals in such systems. The time required to calculate correlated wavefunctions with multi-reference and/or CI methods therefore scales steeply with the number of electrons, and limits their application in studying interesting transition metal systems.

3.5. Defining a basis set for ab initio calculations on transition metal complexes

Although the equations above are formulated in terms of the spin orbitals of the open-shell system, these MOs are usually expanded in terms of hydrogen-like atomic orbitals, such that:

$$\varphi_i = \sum_{\mu=1}^{N} c_{\mu i} \phi_{\mathrm{u}}$$

The linear combination of atomic orbitals (LCAO) to describe the unrestricted MOs requires the definition of a basis set of hydrogenic functions (s, p, d, f and so on). Unfortunately, an infinite number of atomic orbitals are required to completely span the space of the electronic structure of a given system, and so the use of a finite basis set constitutes another approximation in obtaining the molecular wavefunction. For the sake of computational simplicity, basis sets are usually constructed from Gaussian-type functions, which take the following general form when centered on an atom a:

$$N x_a^i y_a^j z_a^k \mathrm{e}^{-\alpha r^2}$$

where N is a normalization constant, and the sum of the non-negative integer variables i, j and k corresponds to the angular momentum quantum number of the hydrogenic orbital. The orbital exponent is denoted by α, and a given atomic orbital is often represented by a linear combination of many Gaussian-type functions.

The selection of the basis set used to construct the unrestricted MOs will clearly influence the level of computational accuracy, and there are a bewildering number of basis sets that have been developed to model the properties of complex molecules [95,109]. In many cases, so as to model geometries correctly, basis sets must contain polarization functions [110–112], and efforts to compute the properties of anionic systems usually require the use of additional diffuse functions. While increasing the accuracy of any molecular wavefunction, the inclusion of additional basis functions, however, significantly increases the computational demand of HF calculations due to n^4-dependence of the number of two-electron integrals that must be evaluated (n is the number of basis functions). Studies of transition metal complexes are a particular problem given the large number of basis functions that must be included to model the non-valence electrons in the metal. As a result, the inner electron shells of transition metals are often represented by effective core potentials (ECPs) [113,114]. These ECPs not only reduce the computational demands of calculations on transition metal systems but they also allow the inclusion of relativistic effects, which are important in the chemical properties of second- and third-row metals, in a straightforward manner.

It is an unfortunate fact that the choice of basis set can have a significant impact upon the outcome of calculations upon metalloenzyme centers, as illustrated in a recent systematic study of the interaction between oxygen and heme complexes [115], raising the issue of how to choose an appropriate basis for a given calculation. Clearly, the inclusion of more basis functions will usually improve the accuracy of the computed properties but at a significant increase in computational cost. The question is further complicated by the software package that is employed to perform the calculations. For example, the implementation of a given basis set may radically affect computational efficiency. One strategy in selecting an appropriate basis for the calculations is to examine the dependence of the proper-

ties computed for small transition metal complexes upon increasing the size of the basis set [116]. An alternative method is to delineate the successes and failures of a specific basis set in calculations on related systems [95], although this approach is often precluded by an insufficient number of previous studies.

4. The meaning of spin contamination in DFT calculations

4.1. The relationship between HF and DFT

Given the computational problems associated with the application of ab initio MO-based methods to problems of structure and reactivity in transition metal-containing complexes, most theoretical studies in this area employ DFT methods [117–119]. DFT calculations take advantage of the fact that the ground-state electronic properties of a molecular system can be determined uniquely not by explicit consideration of a wavefunction but by the electron density alone [120,121]. Thus, the molecular properties are functionals of $\rho(\mathbf{r})$ because ρ itself is a function of the spatial coordinates, x, y, and z. It can be shown that the ground-state energy is variational with respect to the electron density $\rho(\mathbf{r})$, and hence the minimum of the ground-state energy functional $E[\rho]$ yields the exact ground-state energy. Unfortunately, the fundamental theorems that underpin the DFT approach provide neither a method for calculating the energy or any other electronic property from the density $\rho(\mathbf{r})$ nor do they define how to determine $\rho(\mathbf{r})$. One solution to this problem is to define the ground-state electronic energy of an N-electron system in terms of the density $\rho(\mathbf{r})$ according to the following expression [122]:

$$E[\rho] = E_{\mathrm{T}}[\rho] + E_{\mathrm{NE}}[\rho] + E_{\mathrm{J}}[\rho] + E_{\mathrm{XC}}[\rho]$$

where $E_{\mathrm{T}}[\rho]$ is the kinetic energy of the electrons, $E_{\mathrm{NE}}[\rho]$ is the nuclear–electron attraction, $E_{\mathrm{J}}[\rho]$ is the Coulombic repulsion between the electrons, and $E_{\mathrm{XC}}[\rho]$ is the exchange–correlation energy, which includes the contributions from both electron exchange and correlation. In this equation, the energy contribution from dynamic and static electron correlation [123] is introduced, albeit in an approximate manner, by defining an effective local 'exchange–correlation' (XC) functional. The extent to which correlation energy is modeled correctly, however, depends on the actual form of the XC functional. Although this energy decomposition is formally exact, the actual expressions for the many-body exchange and correlation interactions in molecules are unknown, leaving the form of the exchange–correlation term unsolved for systems of chemical interest. Writing the energy dependence on electron densities in a more explicit form leads to the following equation:

$$E[\rho] = T_{\mathrm{S}}[\rho] + \int \mathrm{d}r\ v(r)\rho(r) + \frac{1}{2}\iint \mathrm{d}r\ \mathrm{d}r' \frac{\rho(r)\rho(r')}{|r - r'|} + E_{\mathrm{XC}}[\rho]$$

There is a one-to-one correspondence between the terms of the last two equations. Thus, the first term describes the kinetic energy of the electrons, and the interaction between the electrons and an external potential (which is the nuclear field in the absence of other potentials) is given by the second term. The final terms are an explicit Coulomb term of known form, and a functional that accounts for both exchange and correlation effects. The last term, which replaces explicit non-local exchange integrals in HF theory by an effective local 'exchange–correlation' functional, is an important feature of DFT. Technically, energy in the DFT formalism depends only on spatial or spin densities. In implementing the method, however, we mentally graft the idea of individual particles occupying MOs to obtain these densities, and retain the Coulomb integrals of HF theory (third term) to account for charge–charge repulsion over the electron densities. The XC functional therefore replaces the exchange integrals that arise in HF theory, and in its 'proper' form will, by definition, give the exact ground state total density and the correct energy even though this effective potential is not evaluated by integrals over every conceivable electron pair, being dependent only on the sum of electron, or electron-spin, density at a given point in space. In addition, this potential includes the effects of electron correlation on the density. Thus, the calculated density behaves as if it were composed of particles that repel each other, both on average (the Coulomb term) and individually (the correlation functional), and which exhibit QM exchange interactions without the need to consider explicit electrons! As a result, removing the electrons from the physical model allows the explicit electron–electron interactions (exchange and correlation) to be described locally in space, an almost unbelievable transformation. Unfortunately, although the existence of this XC functional can be proved, its explicit form that is required for calculations on systems of chemical interest has not been determined. Thus, the grueling evaluation of four-center/two-electron integrals and lack of electron correlation in HF theory has been replaced by the need to find approximations for the 'unknown' XC effective potential.

One method of overcoming this dilemma is to introduce ideas from MO theory. Using the orbital-dependent kinetic energy operator, gives the following Kohn-Sham (KS) equation:

$$\left[-\frac{1}{2}\nabla^2 + v(r) + \int \mathrm{d}r' \frac{\rho(r')}{|r - r'|} + V_{\mathrm{XC}}(\rho(r))\right]\psi_i(r) = \varepsilon_i\psi_i(r)$$

in which the density $\rho(\mathbf{r})$ is constructed from a basis set of orbitals:

$$\rho(r) = \sum_{i=1}^{N} |\psi_i(r)|^2$$

At first glance, the DFT equations resemble those of HF theory, which were described above. There is a critical difference in the model single-determinant wavefunctions that are used in each method, however, because DFT considers a system of non-interacting electrons. As a consequence of this model, and unlike HF theory, which includes specific two-electron integrals to introduce the effects of Coulombic repulsion, the explicit interactions between electrons are not present in the KS equations. The N-particle KS equation therefore becomes a single-particle equation in which the model single determinant wavefunction, Φ_S, is constructed from KS MOs, φ_i, which are defined such that:

$$\rho(x,\ y,\ z) = \rho(\vec{r}) = \sum_{i}^{n} \varphi_i^*(\vec{r})\varphi_i(\vec{r})$$

Note that the KS orbitals are not identical to HF orbitals [124], although it has been demonstrated that the spatial distribution of both sets of MOs is very similar [125]. All of the electron–electron interactions are therefore included implicitly in the effective single-particle potential. According to the basic theorems of DFT [122], if the interacting and non-interacting systems have the same ground-state electron density, then the external potentials must be identical and are uniquely determined from the density. The assumption of the existence of a non-interacting system with the exact ground-state density corresponding to an anti-symmetric, ground state wavefunction, is termed v-representability.

In principle, these equations can be used to obtain molecular excited states of different symmetry to the ground state subject to the constraint that a given excited state wavefunction is orthogonal to the wavefunctions of the ground state and all other excited states that are lower in energy. It is not, however, necessarily true that DFT wavefunctions of different symmetry will have the same form of the KS potential, and DFT is therefore generally considered to be useful only in modeling ground state properties [19].

Since only one-electron integrals and integrals over the density need to be evaluated, these calculations scale as N^3, where N is the number of basis functions, and algorithms can be formulated to yield 'linear-scaling', or 'divide-and-conquer' methods [126,127]. As a result, DFT represents an ideal QM approach for computing the electronic properties of transition metal complexes, given the need to use large basis sets and to include correlation. On the other hand, an exchange–correlation potential, $V_{XC}(\rho)$ must be formulated in terms of the electron density, without an explicit strategy for solving this problem. This has lead to the development of many competing exchange–correlation functionals that yield molecular properties of varying degrees of accuracy. As a pedagogical point, we note that the actual implementations of density functionals in different electronic structure packages may differ, complicating efforts to replicate literature calculations.

4.2. MOs and electron density

For most chemists, the power of computational methods lies in our ability to rationalize bonding and reactivity in terms of MOs [128]. DFT calculations, however, yield only the electronic density corresponding to the ground-state wavefunction, assuming that the density is v-representable. There are two problems, however, that prevent us from equating the density computed by DFT for a non-interacting system of electrons with a determinantal wavefunction, such as that used in HF theory. First, we cannot guarantee that a given trial density, required as part of the variational procedure that is used to obtain the converged ground-state density, will satisfy v-representability because we do not a priori know the conditions for obtaining a v-representable density! On the other hand, because our trial density is positive everywhere in space, adds up to the proper number of electrons in the chemical system, and is continuous, the density is N-representable and can, in principle, be expressed as a single Slater determinant of N MOs [119]. The second problem, however, is more pernicious. In DFT, the energy of a molecular system depends only on the electron density. This presents the inorganic chemist with a conundrum: how do we arrive at a MO picture of a transition metal complex when the energy depends only on the density? As outlined above, one can define a set of KS orbitals that yield the observed density. This definition, however, gives only a single-determinantal description of the system, which does not formally describe realistic chemical systems that should be represented by a linear combination of many Slater determinants of MOs. Even if we have the exact, universal spin-density functional, it is not therefore clear how we can either obtain a unique linear decomposition of the density into the Slater determinants representing the molecular wavefunction, or reconcile the single determinant of KS orbitals with any multi-determinantal decomposition (Fig. 4). Nevertheless, we note that even with this reservation, the KS orbitals appear to be as robust as HF orbitals for qualitative interpretation and rationalization of molecular properties [129].

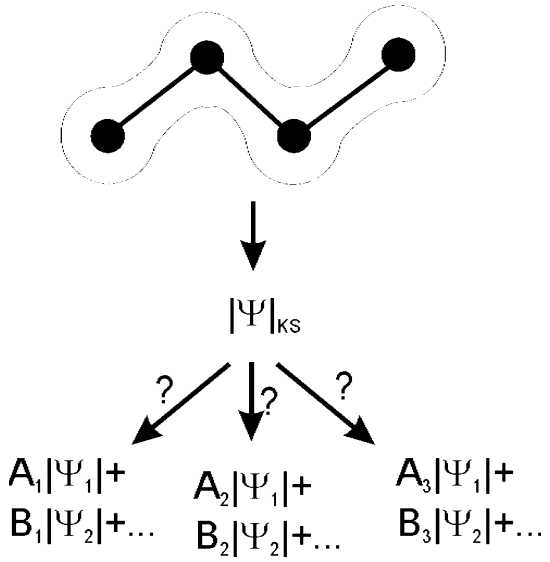

Fig. 4. By requiring N-representability, the density in DFT can be represented by a single determinant composed of KS orbitals, which is analogous the Slater determinant used in HF calculations. The 'true' molecular wavefunction, however, must be described by multiple determinants, and there is no unique decomposition of the KS determinant or the corresponding density. A_x, B_x represent coefficients, and Ψ_x the component Slater determinants in a multi-determinantal expansion of the molecular wavefunction.

4.3. DFT methods for computing the properties of open-shell Fe(III) systems

Density functional methods generally differ in how the exchange–correlation (XC) functional is approximated. Early efforts to develop suitable XC functionals were based only on electron density [122,130]. In DFT calculations on open-shell systems, which must employ the local spin density approximation (LSDA), the local exchange–correlation energy depends not only on the electron density, but also on the spin magnetization density, i.e. the difference between the electron density of α- (ρ^{α}) and β-spin electrons (ρ^{β}) [131]. Improvements to this approach, which often underestimates the contribution of exchange energy [132], require the inclusion of gradient-corrections to the density [133–135]. The BLYP method, one of the most commonly used DFT models, combines a gradient-corrected exchange functional (B88) [132], which correctly models the asymptotic potential of the exchange-energy and spin densities, with the gradient-corrected Lee–Yang–Parr (LYP) correlation functional [136]. More recently, advances in DFT have centered on hybrid functionals in which the exchange energy of a molecular system is evaluated using a weighted sum of orbital-dependent (HF) exchange integrals and a DFT exchange functional. A particularly important development was B3PW91, a three-parameter functional expression including the PW91 correlation functional [133], which reproduced experimental heats of formation [137]. Subsequently, this functional was modified by the inclusion of the LYP functional [136] to give the B3LYP method [138], and DFT calculations on transition metal complexes using this model have generally given excellent results [10]. Experimental chemists seeking to employ B3LYP in calculations on Fe(III)-containing systems should, however, take care because different software packages employ alternate formulations of the method and hence yield different absolute and relative energies for a given molecular system. For example, B3LYP is implemented in the GAUSSIAN-98 package [139] according to the following expression:

$$F^{\mathrm{B3LYP}} = (1-A)F_{\mathrm{x}}^{\mathrm{Slater}} + AF_{\mathrm{x}}^{\mathrm{HF}} + BF_{\mathrm{x}}^{\mathrm{Becke}} + CF_{\mathrm{c}}^{\mathrm{LYP}} + (1-C)F_{\mathrm{c}}^{\mathrm{VWN}}$$

where $F_{\mathrm{x}}^{\mathrm{Slater}}$ and $F_{\mathrm{x}}^{\mathrm{HF}}$ represent Slater exchange and exact HF exchange, respectively, and $F_{\mathrm{x}}^{\mathrm{Becke}}$ is the gradient-corrected, B88 exchange functional [132]. $F_{\mathrm{c}}^{\mathrm{LYP}}$ and $F_{\mathrm{c}}^{\mathrm{VWN}}$ correspond to the correlation functionals of LYP [136], and Vosko–Wilk–Nusair (VWN) [130], respectively. In the TURBOMOLE program [140], however, a different version of the VWN correlation functional is employed. In our experience, while the B3LYP energies computed for Fe(III)-containing systems using GAUSSIAN-98 and TURBOMOLE differ in their absolute values, relative spin state energies generally differ by less than 1 kcal. This is well within the errors of this DFT method. There is therefore no clear reason to favor one of these B3LYP implementations over the other in studies of Fe(III) complexes, but DFT calculations employing the B3LYP model should be performed using a single functional form if reliable comparisons are to be made.

4.4. Evaluating spin-state properties and spin contamination in DFT calculations

Once the ground-state density has been determined, it is possible to calculate any molecular properties that depend explicitly on the density. However, it is common to calculate other properties that do not depend on the density by simply taking the expectation value of the non-interacting model KS determinant. Properties calculated in such fashion do not correspond to those of the interacting system, but rather to the non-interacting model system [141]. One example is the total spin angular momentum, $\langle \hat{S}^2 \rangle$, which is a two-particle property, and indicates the amount of spin contamination in the wavefunction computed for open-shell systems such as Fe(III) complexes. The interpretation of spin contamination in UHF wavefunctions is relatively straightforward, because the Fock operator takes explicit account of two-particle interactions in the Coulomb and exchange integrals. It is less clear whether similar information can be obtained concerning the

amount of spin contamination present in 'wavefunctions' obtained for open-shell transition metal complexes using DFT methods, in which the exchange interaction is collapsed into an effective one-particle potential depending on the density at a point in space. This is obviously an important problem in evaluating the spin state-dependent properties of Fe(III) complexes that are of chemical interest because DFT calculations represent the only practical approach to computing the electronic structure of such compounds with reasonable accuracy. Some workers have dismissed the possibility of correctly estimating two-particle properties from a KS determinant [19,142]. It has also been argued that spin contamination in KS reference wavefunctions should be ignored [143]. Since the calculated density computed by DFT methods is N-representable, however, we consider the KS orbitals to provide the best single-determinant description of the system within the limitations of the basis set of orbitals used in performing the calculation. While conceding that this is an inexact description of a wavefunction that is inherently multideterminantal in nature, the same objection can be raised against the UHF wavefunctions that are used to model open-shell systems. We therefore conclude that KS orbitals are as suitable for evaluating two-particle properties as the MOs obtained in any HF calculation that does not include the effects of electron correlation, and note that others have supported the concept that KS orbitals represent physically meaningful entities [125]. From this perspective, several studies using the non-interacting formulation for $\langle \hat{S}^2 \rangle_{KS}$ have indicated that DFT wavefunctions computed for organic molecules do not tend to suffer from substantial amounts of spin contamination [144–148], and that non-interacting values of $\langle \hat{S}^2 \rangle_{KS}$ are only slightly larger than those computed for the full, interacting system [149].

4.5. Practical aspects of evaluating spin-state properties using DFT calculations

In performing any DFT calculation, the user must specify: (i) the computational method (e.g. B3LYP) and atomic basis; (ii) the initial molecular geometry and composition; (iii) the total charge on the system; and (iv) the spin multiplicity of any open-shell system, which is specified in the calculation by $2S_z+1$, not $2S+1$! When using crystal structures in our DFT calculations, counterions and solvent molecules observed in the crystal are not usually included. The SCF calculation to obtain the density requires an initial guess for the orbitals and coefficients, which is often obtained from a simple extended Hückel calculation [150] as the default option in many software packages. In our experience, however, avoiding convergence problems in DFT calculations on Fe(III) complexes requires a set of initial densities obtained from UHF calculations, using either a STO-3G or 3-21G* basis [109]. The KS equations are then solved self-consistently to obtain a new set of densities, and the process is repeated until convergence is achieved. In our studies, we usually require that the density matrix be converged to a tight rms threshold of 1.0×10^{-8} in all single point energy determinations. In addition, we routinely perform a stability check to ensure that the DFT 'wavefunction' is converged to a minimum energy solution. This is especially important for calculations on Fe(III)-containing complexes for which there are usually a manifold of electronic states that differ in chemical properties but are close in energy [10].

Within a single-determinantal theory, an unrestricted formalism allows the most realistic description of transition metal complexes. If $\langle \hat{S}^2 \rangle$ is close to the ideal value, the unrestricted calculation should give reasonably accurate relative spin state energies (the absolute differences, however, will depend on the accuracy of the method). If $\langle \hat{S}^2 \rangle$ deviates greatly from ideal, then a restricted open-shell calculation can give reasonable descriptions of at least the highest S_z component of a spin manifold. Since in the absence of zero-field splitting or a magnetic field the S_z states are degenerate, this may be good enough to determine spin state energies, even though spin polarization is neglected. In systems with appreciable spin–orbit coupling, further measures beyond the scope of this review must be considered to give an accurate description of the ground-state electronic structure.

5. Computing the spin-dependent properties of non-heme Fe(III) complexes

5.1. Previous theoretical investigations of mononuclear Fe-containing complexes

Few systematic DFT investigations of spin state preferences in mononuclear Fe-containing molecules have been reported [16,93,151–161], and these studies have yielded mixed results. For example, while the spin preferences of $Fe(CO)_3^+$, $Fe(CO)_4^+$, and $Fe(CO)_5^+$ are correctly modeled by DFT calculations [151], wavefunctions computed using the B3LYP functional were reported to exhibit a bias towards high spin-states for complexes between Fe and dioxygen [16,152]. DFT calculations have also been employed to determine the relative spin-state energetics of the Fe(II) anti-cancer drug bleomycin [153], Fe(II) porphyrins [93,154,155], and Fe-containing models of deoxyheme [156], and the active site of cytochrome P_{450} [157–159]. These studies were, however, employed as predictive tools to determine ground state spin preferences and relative spin-state energetics, and generally were not calibrated by direct comparison to experimental data. In an impor-

tant, but relatively limited, study of the mononuclear, non-heme Fe(III) complex $Fe(H_2O)_6^{3+}$, DFT methods were shown to reproduce the experimental ordering of spin-states [160], and to give results that were comparable to those obtained using other theoretical methods. The same study also demonstrated the reliability of INDO/S semiempirical method [162,163] in characterizing the electronic properties of Fe(III) complexes, a conclusion that has been supported by recent success in using projection UHF-INDO/S (PUHF-INDO/S) calculations [101,102] to model the properties of model NHase Fe(III) complexes [164]. The application PUHF/INDO/S methods to model the catalytic mechanism of NHase is, however, precluded by the lack of optimized structures for putative intermediates that might mediate the hydration reaction. Since DFT calculations represent the only practical method for computing the structural properties of the NHase active site and these intermediates, our group has explored the ability of various functionals to model the electronic structure and spin preferences of selected model NHase Fe(III) complexes prior to applying this theoretical approach to studies of the enzyme itself.

5.2. *In vacuo* DFT studies of NHase model Fe(III) complexes

A series of non-heme Fe(III) complexes have been prepared that provide a starting point for investigating the chemical and physical properties of the metal when it is coordinated by a mixed set of sulfur and nitrogen-containing ligands [64]. The availability of high-resolution crystal structures for many of these complexes [165], together with data upon their spin properties and UV–vis spectra, presents an ideal opportunity to calibrate DFT methods in modeling the spin preferences and electronic structures of non-heme, Fe(III)-containing systems [166], and to assess the extent of spin contamination in such calculations. Recent results suggest that gas-phase DFT calculations employing the B3LYP functional correctly reproduce the observed ground state spin preferences of these Fe(III) complexes, and that there is relatively little spin contamination thereby allowing an assessment of spin state-dependent effects on molecular structure. For example, the Fe(III) complex **1** [67] (Fig. 5) is a particularly good model of the NHase center because the metal is coordinated by deprotonated amide nitrogen and thiolate ligands in an octahedral environment, and prefers a doublet ($S = 1/2$) ground state. At the crystal geometry, DFT calculations employing either the BLYP or B3LYP [135] functionals, in combination with a 6-31G* basis [167–169], correctly predict the ground state spin preference for **1** without any significant amount of spin contamination (Table 1) on basis of the non-interacting value of $\langle \hat{S}^2 \rangle_{KS}$. In order to ensure that there was no systematic bias of the

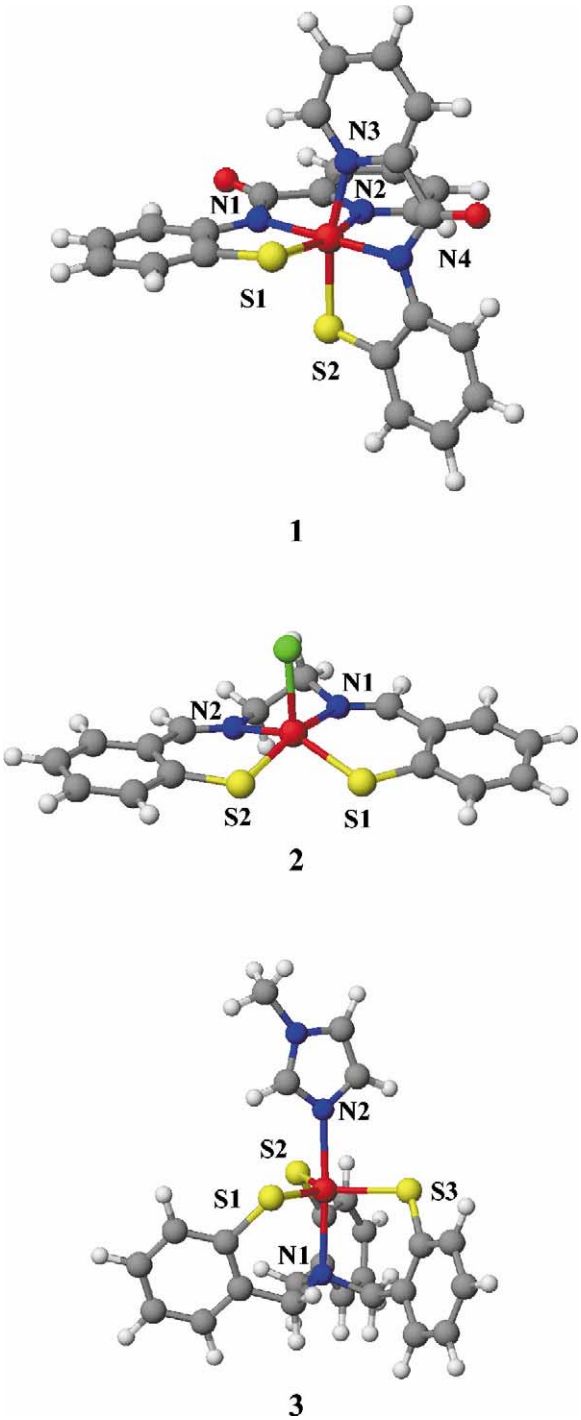

Fig. 5. X-ray crystal structures of Fe(III) complexes **1**–**3**. **1**, [Fe^{III}(PyPepS)$_2$], where PyPepSH = *N*-2-mercaptophenyl-2′-pyridinecarboxamide; **2**, [Chloro-(*N*,*N*′-ethylenebis(thiosalicylideneiminato)Fe^{III}]; **3**, [Fe^{III}(N{CH_2–*o*-C_6H_4S}$_3$)(1-Me–Imid)]. Atoms are colored using the following scheme: C, grey; H, white; N, blue; O, red; S, yellow; Fe, orange; Cl, green.

method towards low spin states, we have also studied Fe(III) complexes, such as **2** [170] and **3** [171] (Fig. 5), which exhibit different ground state spin preferences, net charge and coordination geometries [166]. Calculations employing the B3LYP functional again predicted

Table 1
Relative spin state energies (cm^{-1}) and the associated non-interacting $\langle \hat{S}^2 \rangle_{KS}$ values of Fe(III) complexes **1**–**3** computed at their experimental geometries using DFT methods

Complex [a]	Spin multiplicity (S_z)	BLYP/6-31G*			B3LYP/6-31G*		
		Relative energy (cm^{-1})	$\langle \hat{S}^2 \rangle_{KS}$ [b,c]	$2S+1$	Relative energy (cm^{-1})	$\langle \hat{S}^2 \rangle_{KS}$ [b,c]	$2S+1$
1	1/2	0	0.77	2.02	0	0.78	2.03
	3/2	10 560	3.81	4.03	8040	3.81	4.03
	5/2	18 830	8.77	6.00	11 560	8.77	6.01
2	1/2	1860	1.20	2.41	4420	1.48	2.63
	3/2	0	3.79	4.02	0	3.82	4.03
	5/2	9020	8.76	6.00	6050	8.76	6.00
3	1/2	0	0.96	2.20	5870	1.18	2.39
	3/2	90	3.82	4.03	3040	3.89	4.07
	5/2	640	8.76	6.00	0	8.76	6.00

[a] Counterions were not included in these calculations.
[b] These are non-interacting $\langle \hat{S}^2 \rangle$ values of the converged DFT wavefunction.
[c] $2S+1 = (4\langle \hat{S}^2 \rangle + 1)^{1/2}$. The values of $\langle \hat{S}^2 \rangle_{exact}$ expected for spin uncontaminated wavefunctions are therefore 0.75, 3.75 and 8.75 for the doublet, quartet and sextet states, respectively [99].

ground state spin state preferences for these complexes at their crystal geometries that were in agreement with experimental data (Table 1), although BLYP calculations predicted that the doublet rather than the observed sextet would be the ground state for complex **3**. The small energy differences between each of the spin states of **3** that were computed using BLYP are within the error of the method [172,173], and therefore preclude the general statement that this functional cannot be employed to model the spin preferences of other Fe(III) complexes. In addition, primarily for reasons of computational difficulty, these energies did not include corrections for differences in the zero point energy of each Fe(III) complex at a specific spin state, given the computational effort and the likelihood that these corrections would be small [160,161]. In contrast to the case of complex **1**, there was significant spin contamination when single-point energy calculations were performed for complexes **2** and **3** at the low-spin state (Table 1) [166]. Given that these latter two Fe(III) complexes prefer quartet [170] and sextet [171] spin configurations, respectively, at the crystal geometries used in these calculations, it seems likely that the doublet states of these complexes are contaminated by higher spin states.

We [166], and others [160], have also investigated whether the effects of spin state on molecular geometry can be adequately modeled by in vacuo geometry optimizations using DFT methods. In general, DFT-optimization of the model NHase Fe(III) complexes yields spin state-specific structures that are consistent with the predictions of metal–ligand bonding and ligand field theory [174,175] (Table 2). If the geometry optimization is performed for a specific Fe(III) complex at its observed spin state, then there is usually a high similarity between the optimized structure and that seen experimentally (Fig. 6). This is particularly true for complex **1** in which the metal ligands closely resemble those seen in the NHase metal center [64]. In an apparent exception to this finding, the Fe–N bonds in the DFT optimized high spin ($S = 5/2$) structure of complex **3** were longer than those present in the crystal, and the pucker of the rings in the ligand was noticeably different (Fig. 6: **3C**). Crystal packing effects undoubtedly influence the experimental geometry observed for the rings of the ligand in complex **3**, emphasizing the need to include the effects of the local environment in these calculations. Efforts to obtain an in vacuo BLYP optimized structure for the quartet spin state of complex **1** were frustrated by problems of SCF convergence that could not be resolved by any of our usual strategies for obtaining good initial guesses of the density. This may reflect the fact that crystal structure, which was used as the initial geometry in the calculation, is too far from that of the optimized quartet.

Although there is no data with which to calibrate the theoretical results, it seems that BLYP/6-31G* optimization of Fe(III) complexes **1**–**3** at spin multiplicities other than the ground state does yield structural changes that are consistent with ligand field theory. For example, an increase of the metal–ligand bond lengths is observed for the high spin state of complex **1** relative to those in the initial, low spin structure. In the case of a square pyramidal complex, such as **2**, stabilization of a high spin state relative to the preferred quartet requires a decreased energetic splitting of the A_1 and B_1 orbitals. Simple ligand field models predict that this change in orbital separation can be achieved by shortening the axial metal–ligand bond (raising the A_1 orbital energy) with concomitant lengthening of the remaining ligand

Table 2
Selected spin state-dependent structural parameters in the optimized BLYP/6-31G* geometries of the Fe(III) complexes **1**–**3** [a]

Complex	Property	Crystal [b]	Initial [c]	$S = 1/2$	$S = 3/2$	$S = 5/2$
1	Fe–S1	2.2284(10) Å	2.227 Å	2.29 Å	– [d]	2.41 Å
	Fe–S2	2.2297(11) Å	2.230 Å	2.29 Å	– [d]	2.41 Å
	Fe–N1	1.954(2) Å	1.955 Å	1.97 Å	– [d]	2.12 Å
	Fe–N2	1.997(2) Å	1.998 Å	1.98 Å	– [d]	2.27 Å
	Fe–N3	2.003(3) Å	2.003 Å	1.98 Å	– [d]	2.26 Å
	Fe–N4	1.954(2) Å	1.955 Å	1.97 Å	– [d]	2.11 Å
	S1–Fe–N2	165.78(8)°	165.8°	167.2°	– [d]	155.9°
	S2–Fe–N3	166.67(8)°	166.7°	167.0°	– [d]	155.9°
	N1–Fe–N4	178.84(10)°	178.8°	179.2°	– [d]	172.8°
2	Fe–Cl	2.336(5) Å	2.336 Å	2.26 Å	2.31 Å	2.25 Å
	Fe–S1	2.196(6) Å	2.195 Å	2.22 Å	2.27 Å	2.37 Å
	Fe–S2	2.187(6) Å	2.187 Å	2.23 Å	2.25 Å	2.37 Å
	Fe–N1	1.98(2) Å	1.980 Å	1.95 Å	1.99 Å	2.15 Å
	Fe–N2	2.03(2) Å	2.031 Å	1.96 Å	2.02 Å	2.15 Å
	S1–Fe–S2	82.3(2)°	82.3°	84.2°	84.3°	88.7°
	N1–Fe–N2	83.4(6)°	83.4°	85.1°	83.9°	78.7°
3	Fe–S1	2.308(4) Å	2.308 Å	2.23 Å	2.31 Å	2.36 Å
	Fe–S2	2.304(5) Å	2.302 Å	2.24 Å	2.36 Å	2.35 Å
	Fe–S3	2.296(5) Å	2.294 Å	2.22 Å	2.39 Å	2.34 Å
	Fe–N1	2.21(1) Å	2.211 Å	2.07 Å	2.04 Å	2.38 Å
	Fe–N2	2.15(1) Å	2.145 Å	2.02 Å	2.03 Å	2.25 Å
	S1–Fe–S2	125.99(9)°	125.6°	127.1°	124.3°	122.9°
	S1–Fe–S3	115.6(2)°	115.6°	105.5°	118.2°	120.3°
	N1–Fe–N2	176.7(5)°	176.7°	176.7°	177.2°	176.9°

Atom numbering corresponds to that shown in Fig. 5.
[a] Counterions were not included in these calculations.
[b] Values in parentheses indicate the standard deviation of the crystallographic measurements.
[c] Bond lengths and angles are those of the initial structure used in the DFT calculations, which differ slightly from those in the crystal structure due to numerical rounding during input file formatting.
[d] The DFT-optimized geometry of complex **1** at this spin state could not be computed due to a lack of SCF convergence for the quartet spin state using the crystal geometry as the initial structure.

bonds (lowering the B_1 orbital energy) [174]. These changes in bond length are observed in the calculated structure of the high spin ($S = 5/2$) form of complex **2** relative to the crystal structure. Equally, shortening the Fe–Cl bond without any changes in the remaining metal–ligand bond lengths should raise the energy of A_1 orbital, thereby increasing the energetic splitting of the A_1 and B_1 orbitals, leading to stabilization of the low spin electronic configuration. Comparison of the BLYP-optimized structures of **2** at the low ($S = 1/2$) and intermediate ($S = 3/2$) spin states reveals the expected decrease in the axial Fe–Cl bond length for the system of lower multiplicity while the remaining ligand bond lengths in the low and intermediate spin complexes are relatively unchanged (Table 2). When the geometry of the trigonal bipyramidal complex **3** was optimized at the intermediate ($S = 3/2$) spin state, there were significant decreases in the axial Fe–N1 and Fe–N2 bond lengths of 34 and 21 pm, respectively, relative to the BLYP-optimized high spin structure (Table 2). These changes are again consistent with that expected from ligand field models in which increased axial metal–ligand interactions in a trigonal bipyramidal complex would raise the A_1' orbital energy to increase the splitting between the E′ and A_1' orbitals. When **3** was optimized at the low ($S = 1/2$) spin state, a decrease in the axial Fe–N bond lengths relative to their values in the high spin structure was accompanied by additional shortening of the remaining metal–ligand bonds. The trigonal arrangement of the equatorial ligands was also distorted due to an increase in the S1–Fe–S2 bond angle. On the basis of ligand field models, such structural changes are associated with the removal of orbital degeneracy that is required in order to attain a low spin multiplicity [174].

Access to in vacuo BLYP-optimized structures for complexes **1**–**3**, permits an evaluation of whether geometry optimization impacts the ability of DFT methods to reproduce experimental spin preferences and the extent of spin contamination (Table 3). Single point energies computed at these optimized geometries using the BLYP functional predicted that complex **3** would adopt a doublet or quartet rather than the

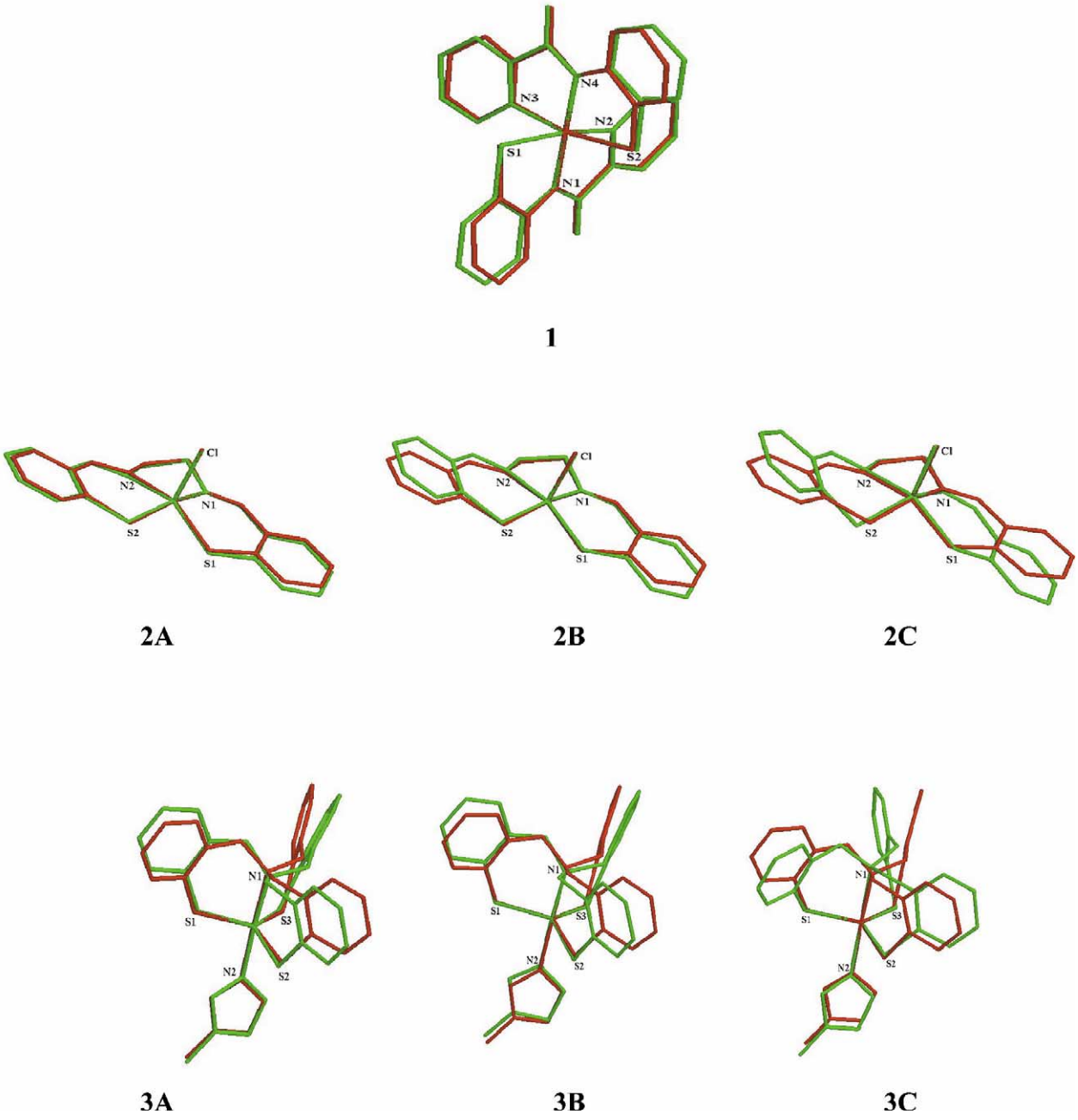

Fig. 6. Superimposition of spin state-dependent BLYP/6-31G* optimized and experimental structures of Fe(III) complexes **1**–**3**. Complexes are colored using the following scheme: red, experimental structure; green, DFT-optimized structure. Structure numbers refer to the electronic configuration at which the complex was optimized, and are as follows: **1**: $S = 1/2$; **2A**: $S = 1/2$; **2B**: $S = 3/2$; **2C**: $S = 5/2$; **3A**: $S = 1/2$; **3B**: $S = 3/2$; **3C**: $S = 5/2$.

observed sextet state. In contrast, similar calculations using the B3LYP functional correctly reproduced the observed spin preferences of these complexes, although the separation of the theoretical quartet and sextet state energies computed using B3LYP for complex **2** are within the error of the method [172,173]. There was also some improvement in the level of spin contamination for the B3LYP wavefunctions describing complexes **2** and **3** in their low spin states for the molecules at their BLYP-optimized rather than experimental geometries.

5.3. Including solvent effects in DFT studies of Fe(III) complexes

Despite the apparent success in using B3LYP/6-31G* calculations to model the spin state energetics of Fe(III) complexes at their in vacuo optimized geometries, there is increasing evidence to suggest that protein environment plays a key role in modulating the chemistry of transition metal centers in enzymes [88,176–179]. Even with the advent of linear-scaling DFT algorithms [126],

Table 3
Relative energies (cm^{-1}) and the associated non-interacting $\langle \hat{S}^2 \rangle_{KS}$ values of Fe(III) complexes **2** and **3** computed at the BLYP/6-31G* optimized geometries at each spin state

Complex [a]	Spin multiplicity (S_z)	BLYP/6-31G*			B3LYP/6-31G*		
		Relative energy (cm^{-1})	$\langle \hat{S}^2 \rangle_{KS}$ [b,c]	$2S+1$	Relative energy (cm^{-1})	$\langle \hat{S}^2 \rangle_{KS}$ [b,c]	$2S+1$
1	1/2	0	0.78	2.03	0	0.79	2.04
	3/2	_ [d]	_ [d]	_ [d]	_ [d]	_ [d]	_ [d]
	5/2	8020 [e]	8.76	6.00	1305 [e]	8.76	6.00
2	1/2	1660	1.02	2.25	5200	1.23	2.43
	3/2	0	3.80	4.02	0	3.84	4.04
	5/2	2800	8.76	6.00	300	8.76	6.00
3	1/2	0	0.76	2.01	4250 [f]	0.91	2.15
	3/2	710	3.79	4.02	1740	3.83	4.04
	5/2	1290	8.76	6.00	0	8.76	6.00

[a] Counterions were not included in these calculations.
[b] These are non-interacting $\langle \hat{S}^2 \rangle$ values of the converged DFT wavefunction.
[c] $2S+1 = (4\langle \hat{S}^2 \rangle + 1)^{1/2}$ [99].
[d] The DFT-optimized geometry of complex **1** at this spin state could not be computed due to a lack of SCF convergence for the quartet spin state using the crystal geometry as the initial structure.
[e] The density matrix and energy for this structure were converged to RMS gradients of 10^{-6} and 10^{-4}, respectively.
[f] The density matrix and energy for this structure were converged to RMS gradients of 10^{-7} and 10^{-6}, respectively.

the size of proteins precludes the use of purely DFT representations in computationally tractable studies. Modeling the transition metal centers of metalloenzymes will therefore require the use of QM/MM simulations if long-range interactions between the metal and protein are to be included in the calculations [180–184]. In this approach, the molecular system is partitioned into a number of regions that are treated by different levels of theory [185]. In the case of NHase, for example, the Fe(III) and its ligands would be described by DFT and the protein/solvent surroundings would be modeled by an empirical, molecular mechanics (MM), potential energy function [186–189]. The effects of the environment are then introduced as steric and electrostatic perturbations in the DFT description of the active site though a coupling potential. Hence, the total energy of system is given by:

$$E_{tot} = E_{QM}(QM) + E_{MM}(MM) + E_{QM/MM}(QM/MM)$$

where $E_{QM}(QM)$ in these calculations is the DFT energy of atoms in the metal center, $E_{MM}(MM)$ is the MM energy of the surroundings, and $E_{QM/MM}(QM/MM)$ is the energy of interaction between the QM and MM subsystems. The latter energy is then defined to be:

$$E_{QM/MM}(QM/MM) = E_{electrostatic}(QM/MM) + E_{vdW}(QM/MM)$$

where $E_{electrostatic}(QM/MM)$ and $E_{vdW}(QM/MM)$ describe the electrostatic and dispersion interactions between the QM and MM regions, respectively. Studies of enzymes are, however, complicated by the need to model bonds between atoms that are described by different potential energy functions (QM or MM) [190–192]. Only a limited number of DFT/MM studies on metal-dependent enzymes have been reported [193–196], and careful calibration of the DFT/MM coupling potentials remains to be performed for metalloenzymes containing mononuclear, non-heme Fe(III) centers, in part because of the computational demands of such calculations.

Environmental effects, including solvation, often play an important role in defining the electronic structure, spectra, and reactivity of solutes [197,198]. Theoretical methods for accurately describing such effects must model both dispersion–repulsion and electrostatic interactions between the solute and solvent, and are therefore best treated by QM/MM methods [199]. Modeling solvent effects on structure and spectroscopy represents a good strategy for calibrating QM/MM coupling potentials, since the solute and solvent can be treated using QM and MM descriptions, respectively. Difficulties that arise from treating covalently bonded QM and MM atoms are therefore avoided. In order to assess the utility of DFT/MM calculations in modeling the NHase active site, the effects of solvation on the molecular geometries, spin preferences and spectroscopy of Fe(III) complexes has been investigated [200] (Fig. 7). We note that there has been relatively little systematic theoretical study of structural differences between transition metal systems in the gas-phase and in condensed phase environments [201–203].

The results of these calculations can be illustrated by DFT/MM geometry optimizations of the NHase model Fe(III) complexes **1** [67] and **3** [171] at their observed spin states in water and DMF, respectively. In these calculations, which employed the TINKER program [204]

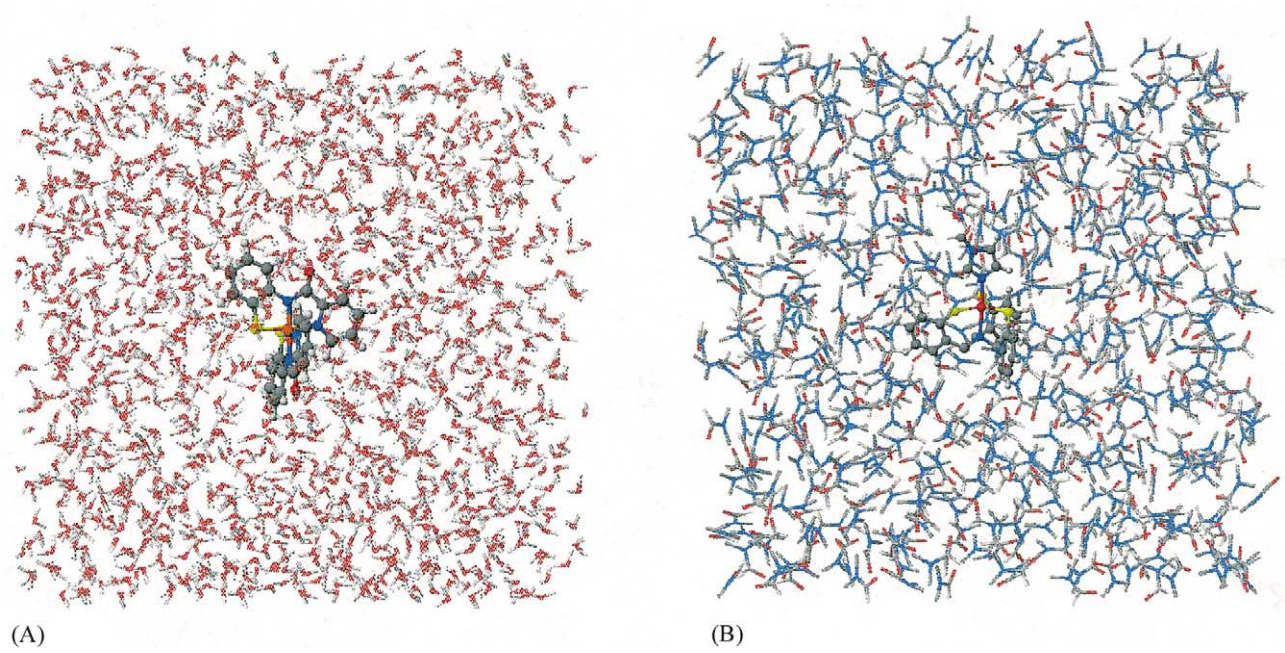

Fig. 7. Computational models of solvated Fe(III) complexes **1** and **3**. (A) Complex **1** surrounded by 1393 H_2O molecules equilibrated at 298 K. (B) Complex **3** surrounded by 487 DMF molecules equilibrated at 298 K. Atoms are colored using the following scheme: C, grey; H, white; N, blue; O, red; S, yellow; Fe, orange. Solvent molecules are rendered as line representations.

Table 4
Relative spin state energies (cm^{-1}) and the associated non-interacting $\langle \hat{S}^2 \rangle_{KS}$ values of Fe(III) complexes **1** and **3** computed at their BLYP/6-31G*/OPLS-A optimized geometries using DFT/MM methods

Complex [a]	Spin multiplicity (S_z)	BLYP/6-31G*/OPLS-A			B3LYP/6-31G*/OPLS-A		
		Relative energy (cm^{-1}) [b]	$\langle \hat{S}^2 \rangle_{KS}$ [c,d]	$2S+1$	Relative energy (cm^{-1})	$\langle \hat{S}^2 \rangle_{KS}$ [c,d]	$2S+1$
1	1/2	0	0.77	2.02	0	0.78	2.03
	3/2	10 160	3.80	4.02	7220	3.81	4.03
	5/2	16 300	4.02	6.00	9200	8.77	6.01
3	1/2	5200	1.22	2.43	10 680	1.33	2.51
	3/2	1960	3.87	4.06	6310	4.04	4.14
	5/2	0	8.76	6.00	0	8.76	6.00

[a] Counterions were not included in these calculations.
[b] Energies correspond to the E_{QM}(QM) portion of the total DFT/MM energy for the solvated complex at the defined spin multiplicity.
[c] These are non-interacting $\langle \hat{S}^2 \rangle$ values of the converged DFT wavefunction.
[d] $2S+1 = (4\langle \hat{S}^2 \rangle + 1)^{1/2}$ [99].

in combination with GAUSSIAN-98, each solute was described by the BLYP functional with a 6-31G* basis, and solvent molecules were modeled using the empirical potential energy functions implemented in the OPLS-A force field [188]. The QM and MM descriptions are coupled using a well-established iterative protocol [192,194]. Thus, ESP charges [205,206] were computed for the Fe(III) complexes at their optimized, gas-phase geometries. These were then employed to equilibrate the solvent molecules about the solute by molecular dynamics (MD) simulation [207], keeping the complex fixed at its initial geometry. Re-optimization of the Fe(III) complex using the BLYP/6-31G* description is then performed keeping the solvent molecules fixed. The influence of the solvent is introduced into these DFT calculations using the QM/MM coupling potential. After convergence of the DFT calculation, the solvent was re-equilibrated at the new geometry of the Fe(III) complex, and the procedure repeated until the total energy (E_{tot}) of the system changes by less than 10^{-6} a.u. between optimization cycles. Single-point E_{QM}(QM) energy components were then computed, using the BLYP/6-31G*/OPLS-A or B3LYP/6-31G*/OPLS-A descriptions, for each of the three spin multiplicities at the DFT/MM optimized geometries of each complex (Table 4). While there was no significant change in the theoretical ordering of spin states in the DFT/MM and DFT gas-phase calculations using the

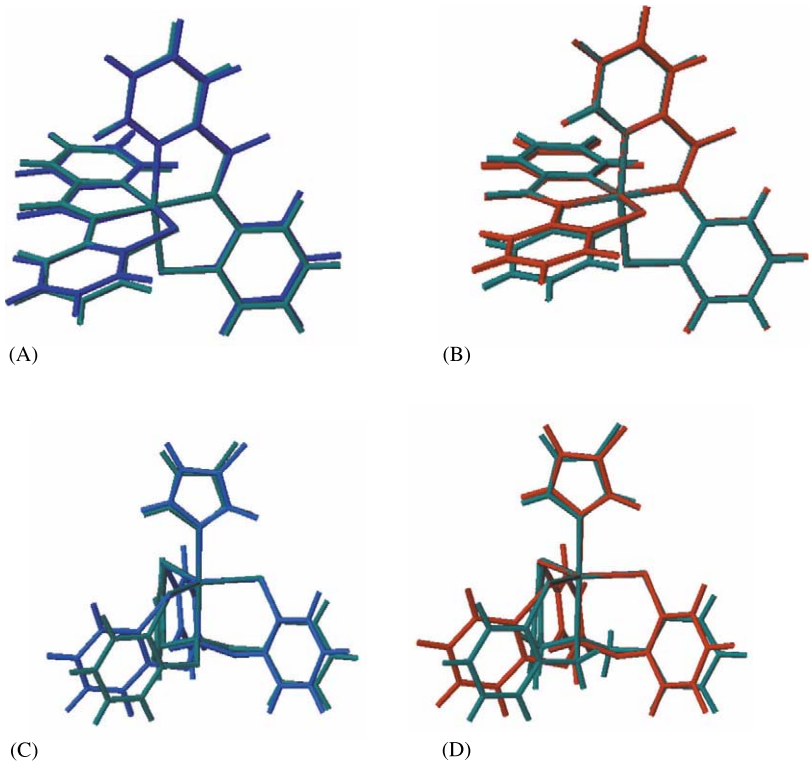

Fig. 8. Superimposition of crystal, BLYP/6-31G* (DFT) and BLYP/6-31G*/OPLS-A (DFT/MM) optimized structures of Fe(III) complexes **1** and **3** at their observed spin states ($S_z = 1/2$ and 5/2, respectively). (A) Superimposed crystal and BLYP/6-31G* geometries of **1**; (B) superimposed crystal and BLYP/6-31G*/OPLS-A geometries of **1**; (C) superimposed crystal and BLYP/6-31G* geometries of **3**; (D) superimposed crystal and BLYP/6-31G*/OPLS-A geometries of **3**. Complexes are colored using the following scheme: crystal geometry, green; in vacuo DFT-optimized geometry, red; DFT/MM-optimized geometry, blue.

B3LYP functional, in vacuo single point energies for **3**, computed at either the crystal or DFT-optimized geometry using the BLYP functional, incorrectly suggested that this Fe(III) complex would exhibit a doublet or quartet rather than the observed sextet state. When the solvent environment was included in the calculation, however, the spin preference of **3** was correctly modeled by the BLYP/6-31G*/OPLS-A single point energies, which were consistent with those computed using the B3LYP/6-31G*/OPLS-A description (Table 4). The level of spin contamination did not appear to be dramatically altered by the inclusion of the QM/MM coupling terms, being comparable to that observed for the gas-phase studies. A comparison of the optimized BLYP/6-31G* and BLYP/6-31G*/OPLS-A geometries for the spin preferred ground state of complex **1** ($S = 1/2$) shows that the inclusion of solvent effects in these calculations did not result in significant changes to either metal–ligand bond lengths or angles (Table 5 and Fig. 8). In contrast, the Fe–S bonds present in the optimized structure of Fe(III) complex **3** have larger values when the effects of the environment are included (Table 5). Whether this difference arises from increased conformational freedom in complex **3** relative to **1** or from the nature of the Fe–N bonds in the two complexes will require further studies involving a larger number of model Fe(III) complexes.

6. Conclusions

DFT calculations, especially those employing the B3LYP functional, on Fe(III) complexes that are models of the NHase metal center are clearly able to yield spin state energies and spin state-dependent structures that are consistent with experimental observations. Since there appears to be relatively little spin contamination in these calculations, at least as measured from the non-interacting value of $\langle \hat{S}^2 \rangle$ for a single determinant of KS orbitals, it appears likely that future DFT studies will be able to provide insight into the role of the carboxamido, and post-translationally modified sulfur, ligands in defining the low-spin character and reactivity of the NHase metal center. The observation that the effects of non-local environment can also be introduced using DFT/MM methods, without any significant increase in spin contamination, also argues that this approach will be useful in examining both the extent to which the protein surroundings modulate Fe(III) reactivity in NHase, and the catalytic mechanism.

Table 5
Selected spin state-dependent structural parameters in the optimized of the Fe (III) complexes **1** ($S = 1/2$) and **3** ($S = 5/2$) in the gas-phase (BLYP/6-31G*) and in solution (BLYP/6-31G*/OPLS-A) [a]

Complex	Property	Initial	BLYP/6-31G*	BLYP/6-31G*/OPLS-A
1	Fe–S1	2.227 Å	2.29 Å	2.27 Å
	Fe–S2	2.230 Å	2.29 Å	2.28 Å
	Fe–N1	1.955 Å	1.97 Å	1.99 Å
	Fe–N2	1.998 Å	1.98 Å	1.99 Å
	Fe–N3	2.003 Å	1.98 Å	1.98 Å
	Fe–N4	1.955 Å	1.97 Å	2.00 Å
	S1–Fe–N2	165.8°	167.2°	167.0°
	S2–Fe–N3	166.7°	167.0°	165.3°
	N1–Fe–N4	178.8°	179.2°	177.7°
3	Fe–S1	2.308 Å	2.23 Å	2.31 Å
	Fe–S2	2.302 Å	2.24 Å	2.36 Å
	Fe–S3	2.294 Å	2.22 Å	2.39 Å
	Fe–N1	2.211 Å	2.07 Å	2.04 Å
	Fe–N2	2.145 Å	2.02 Å	2.03 Å
	S1–Fe–S2	125.6°	127.1°	124.3°
	N1–Fe–N2	176.7°	176.7°	177.2°

Atom numbering corresponds to that shown in Fig. 5.
[a] Counterions were not included in these calculations.

Acknowledgements

Professors Rodney J. Bartlett (University of Florida) and Weitao Yang (Duke University) are gratefully acknowledged for useful discussions about fundamental aspects of molecular spin state calculations and density functional theory. We thank the National Science Foundation (CHE-0079008), the Deutscher Akademischer Austauschdienst (DAAD), and the National Institutes of Health, DHSS (DK61193) for support of this work. Computing resources for this project were provided, under the auspices of the NSF/NPACI program, by the Supercomputing Center at the University of Texas, Austin, and the San Diego Supercomputing Center.

References

[1] L. Noodleman, T. Lovell, T. Liu, F. Himo, R.A. Torres, Curr. Opin. Chem. Biol. 6 (2002) 259.
[2] P.E.M. Siegbahn, Curr. Opin. Chem. Biol. 6 (2002) 227.
[3] P.M. Kozlowski, Curr. Opin. Chem. Biol. 5 (2001) 736.
[4] D.L. Harris, Curr. Opin. Chem. Biol. 5 (2001) 724.
[5] S. Niu, M.B. Hall, Chem. Rev. 100 (2000) 353.
[6] P.E.M. Siegbahn, M.R.A. Blomberg, Chem. Rev. 100 (2000) 421.
[7] G. Frenking, N. Frohlich, Chem. Rev. 100 (2000) 717.
[8] P.E.M. Siegbahn, M.R.A. Blomberg, Annu. Rev. Phys. Chem. 50 (1999) 221.
[9] R.A. Friesner, M.D. Beachy, Curr. Opin. Struct. Biol. 8 (1998) 257.
[10] P.E.M. Siegbahn, Adv. Chem. Phys. 93 (1996) 333.
[11] V.R. Jensen, W. Thiel, Organometallics 20 (2001) 4852.
[12] F. Freeman, M.L. Kassner, W.J. Hehre, J. Phys. Chem. Sect. A 105 (2001) 10123.
[13] S.A. Decker, T.R. Cundari, J. Organomet. Chem. 635 (2001) 132.
[14] P.A. Nielsen, P.-O. Norrby, T. Liljefors, N. Rega, V. Barone, J. Am. Chem. Soc. 122 (2000) 3151.
[15] C. Moberg, U. Bremberg, K. Hallman, M. Svensson, P.-O. Norrby, A. Hallberg, M. Larhed, I. Csöregh, Pure Appl. Chem. 71 (1999) 1477.
[16] G.L. Gutsev, S.N. Khanna, B.K. Rao, P. Jena, J. Phys. Chem. Sect. A 103 (1999) 5812.
[17] A. Görling, S.B. Trickey, P. Gisdakis, N. Rösch, Top. Organomet. Chem. 4 (1999) 109.
[18] T. Ziegler, Chem. Rev. 91 (1991) 651.
[19] A.C. Stückl, C.A. Daul, H.U. Güdel, Int. J. Quant. Chem. 61 (1997) 579.
[20] H.M. Lam, K.T. Coschigano, I.C. Oliveira, R. Melo-Oliveira, G.M. Coruzzi, Annu. Rev. Plant Physiol. Plant Mol. Biol. 47 (1996) 569.
[21] M. Kobayashi, Y. Fujiwara, M. Goda, H. Komeda, S. Shimizu, Proc. Natl. Acad. Sci. USA 94 (1997) 11986.
[22] D.E. Stevenson, R. Feng, F. Dumas, D. Groleau, A. Mihoc, A.C. Storer, Biotechnol. Appl. Biochem. Biotechnol. 15 (1992) 283.
[23] D.M. Stalker, L.D. Malyj, K.E. McBride, J. Biol. Chem. 263 (1988) 6310.
[24] Y. Asano, M. Tachibana, Y. Tani, H. Yamada, Agric. Biol. Chem. 46 (1982) 1175.
[25] I. Endo, M. Nojiri, M. Tsujimura, M. Nakasako, S. Nagashima, M. Yohda, M. Odaka, J. Inorg. Biochem. 83 (2001) 247.
[26] M. Kobayashi, S. Shimizu, Curr. Opin. Chem. Biol. 4 (2000) 95.
[27] I. Endo, M. Odaka, M. Yohda, Trends Biotechnol. 17 (1999) 244.
[28] M. Kobayashi, S. Shimizu, Nat. Biotechnol. 16 (1998) 733.
[29] H. Yamada, M. Kobayashi, Biosci. Biotechnol. Biochem. 60 (1996) 1391.
[30] M. Kobayashi, T. Nagasawa, H. Yamada, Trends Biotechnol. 10 (1992) 402.
[31] M.J. Nelson, H. Jin, I.M. Turner, Jr., G. Grove, R.C. Scarrow, B.A. Brennan, L. Que, Jr., J. Am. Chem. Soc. 113 (1991) 7072.
[32] M.-A. Kopf, D. Bonnet, I. Artaud, D. Pétré, D. Mansuy, Eur. J. Biochem. 240 (1996) 239.
[33] M.S. Payne, S. Wu, R.D. Fallon, G. Tudor, B. Stieglitz, I.M. Turner, M.J. Nelson, Biochemistry 36 (1997) 5447.
[34] Y. Sugiura, J. Kuwahara, T. Nagasawa, H. Yamada, J. Am. Chem. Soc. 109 (1987) 5848.
[35] B.A. Brennan, G. Alms, M.J. Nelson, L.T. Durney, R.C. Scarrow, J. Am. Chem. Soc. 118 (1996) 9194.
[36] L. Que, Jr., R.Y.N. Ho, Chem. Rev. 96 (1996) 2607.
[37] T. Nagasawa, K. Takeuchi, H. Yamada, Eur. J. Biochem. 196 (1991) 581.
[38] M. Kobayashi, M. Nishiyama, T. Nagasawa, S. Horinouchi, T. Beppu, H. Yamada, Biochim. Biophys. Acta 1129 (1991) 23.
[39] M. Nojiri, H. Nakayama, M. Odaka, M. Yohda, K. Takio, I. Endo, FEBS Lett. 465 (2000) 173.
[40] W. Huang, J. Jia, J. Cummings, M. Nelson, G. Schneider, Y. Lindqvist, Structure 5 (1997) 691.
[41] S. Nagashima, M. Nakasako, N. Dohmae, M. Tsujimura, K. Takio, M. Odaka, M. Yohda, N. Kamiya, I. Endo, Nat. Struct. Biol. 5 (1998) 347.
[42] A. Miyanaga, S. Fushinobu, K. Ito, T. Wakagi, Biochem. Biophys. Res. Commun. 288 (2001) 1169.

[43] B.A. Brennan, J.G. Cummings, D.B. Chase, I.M. Turner, Jr., M.J. Nelson, Biochemistry 35 (1996) 10068.
[44] R.C. Scarrow, B.A. Brennan, J.G. Cummings, H. Jin, D.J. Duong, J.T. Kindt, M.J. Nelson, Biochemistry 35 (1996) 10078.
[45] H. Jin, I.M. Turner, Jr., M.J. Nelson, R.J. Gurbiel, P.E. Doan, B.M. Hoffman, J. Am. Chem. Soc. 115 (1993) 5290.
[46] J.W. Peters, M.H.B. Stowell, S.M. Soltis, M.G. Finnegan, M.K. Johnson, D.C. Rees, Biochemistry 36 (1997) 1181.
[47] M. Tsujimara, N. Dohmae, M. Odaka, M. Chijimatsu, K. Takio, M. Yohda, M. Hoshino, S. Nagashima, I. Endo, J. Biol. Chem. 272 (1997) 29454.
[48] T. Murakami, M. Nojiri, H. Nakayama, M. Odaka, M. Yohda, N. Dohmae, K. Takio, T. Nagamune, I. Endo, Protein Sci. 9 (2000) 1024.
[49] S.R. Piersma, M. Nojiri, M. Tsujimura, T. Noguchi, M. Odaka, M. Yohda, Y. Inoue, I. Endo, J. Inorg. Biochem. 80 (2000) 283.
[50] T. Nagasawa, K. Ryuno, H. Yamada, Biochem. Biophys. Res. Commun. 139 (1986) 1305.
[51] C.A. Grapperhaus, A.K. Patra, M.S. Mashuta, Inorg. Chem. 41 (2002) 1039.
[52] J.C. Noveron, M.M. Olmstead, P.K. Mascharak, J. Am. Chem. Soc. 123 (2001) 3247.
[53] L.A. Tyler, J.C. Noveron, M.M. Olmstead, P.K. Mascharak, Inorg. Chem. 39 (2000) 357.
[54] D.S. Marlin, M.M. Olmstead, P.K. Mascharak, Inorg. Chim. Acta 297 (2000) 106.
[55] J. Shearer, I.Y. Kung, S. Lovell, W. Kaminsky, J.A. Kovacs, J. Am. Chem. Soc. 123 (2001) 463.
[56] H.L. Jackson, S.C. Shoner, D. Rittenberg, J.A. Cowen, S. Lovell, D. Barnhart, J.A. Kovacs, Inorg. Chem. 40 (2001) 1646.
[57] I. Kung, D. Schweitzer, J. Shearer, W.D. Taylor, H.L. Jackson, S. Lovell, J.A. Kovacs, J. Am. Chem. Soc. 122 (2000) 8299.
[58] R.C. Scarrow, B.S. Strickler, J.J. Ellison, S.C. Shoner, J.A. Kovacs, J.J. Cummings, M.J. Nelson, J. Am. Chem. Soc. 120 (1998) 9237.
[59] J.J. Ellison, A. Neinstedt, S.C. Shoner, D. Barnhart, J.A. Cowen, J.A. Kovacs, J. Am. Chem. Soc. 120 (1998) 5691.
[60] S. Chatel, M. Rat, S. Dijols, P. Leduc, J.P. Tuchagues, D. Mansuy, I. Artaud, J. Inorg. Biochem. 80 (2000) 239.
[61] M.-A. Kopf, D. Varech, J.-P. Tuchagues, D. Mansuy, I. Artaud, J. Chem. Soc. Dalton Trans. (1998) 991.
[62] L. Heinrich, Y. Li, J. Vaissermann, G. Chottard, J.-C. Chottard, Angew. Chem. Int. Ed. Engl. 38 (1999) 3526.
[63] A.L. Nivorozhkin, A.I. Uraev, G.I. Bondarenko, A.S. Antsyshkina, V.P. Kurbatov, A.D. Garnovskii, C.I. Turta, N.D. Brashoveanu, Chem. Commun. (1997) 1711.
[64] P.K. Mascharak, Coord. Chem. Rev. 225 (2002) 201.
[65] D.S. Marlin, P.K. Mascharak, Chem. Soc. Rev. 29 (2000) 69.
[66] I. Artaud, S. Chatel, A.S. Chauvin, D. Bonnet, M.A. Kopf, P. Leduc, Coord. Chem. Rev. 190–192 (1999) 577.
[67] J.C. Noveron, M.M. Olmstead, P.K. Mascharak, Inorg. Chem. 37 (1998) 1138.
[68] X. Tao, D.W. Stephan, P.K. Mascharak, Inorg. Chem. 26 (1987) 754.
[69] J.C. Noveron, M.M. Olmstead, P.K. Mascharak, J. Am. Chem. Soc. 121 (1999) 3553.
[70] L.A. Tyler, J.C. Noveron, M.M. Olmstead, P.K. Mascharak, Inorg. Chem. 38 (1999) 616.
[71] A. Veillard, Chem. Rev. 91 (1991) 743.
[72] S.R. Langhoff, C.W. Bauschlicher, Jr., Ann. Rev. Phys. Chem. 39 (1988) 181.
[73] D.R. Salahub, M.C. Zerner, in: M.J. Comstock (Ed.), The Challenge of d and f Electrons, American Chemical Society, Washington DC, 1989.
[74] M.W. Schmidt, M.S. Gordon, Annu. Rev. Phys. Chem. 49 (1998) 233.
[75] H.S.R. Gilson, M. Krauss, J. Phys. Chem. Sect. A 102 (1998) 6525.
[76] B.O. Roos, K. Andersson, M.P. Fülscher, P.-Å. Malmqvist, L. Serrano-Andres, K. Pierloot, M. Merchán, Adv. Chem. Phys. 93 (1996) 219.
[77] K. Pierloot, J.O.A. De Kerpel, U. Ryde, B.O. Roos, J. Am. Chem. Soc. 119 (1997) 218.
[78] U. Ryde, M.H.M. Olsson, K. Pierloot, B.O. Roos, J. Mol. Biol. 261 (1996) 586.
[79] A.J.H. Wachters, J. Chem. Phys. 52 (1970) 1033.
[80] K. Ohno, N. Kamiya, N. Asakawa, Y. Inoue, M. Sakurai, J. Am. Chem. Soc. 123 (2001) 8161.
[81] J.J.P. Stewart, Int. J. Quant. Chem. 58 (1996) 133.
[82] W. Thiel, A.A. Voityuk, J. Phys. Chem. Sect. A 100 (1996) 616.
[83] N. Lehnert, R.Y.N. Ho, L. Que, Jr., E.I. Solomon, J. Am. Chem. Soc. 123 (2001) 12802.
[84] M. Wirstam, P.E.M. Siegbahn, J. Am. Chem. Soc. 122 (2000) 8539.
[85] D.M. Ball, C. Buda, A.M. Gillespie, D.P. White, T.R. Cundari, Inorg. Chem. 41 (2002) 152.
[86] T.G. Spiro, M.Z. Zgierski, P.M. Kozlowski, Coord. Chem. Rev. 219 (2001) 923.
[87] S. Li, M.B. Hall, Inorg. Chem. 40 (2001) 18.
[88] B.F. Gherman, B.D. Dunietz, D.A. Whittington, S.J. Lippard, R.A. Friesner, J. Am. Chem. Soc. 123 (2001) 3836.
[89] A. Ghosh, E. Steene, J. Biol. Inorg. Chem. 6 (2001) 739.
[90] P.E.M. Siegbahn, J. Comput. Chem. 22 (2001) 1634.
[91] E.I. Solomon, P. Chen, M. Metz, S.K. Lee, A.E. Palmer, Angew. Chem. Int. Ed. Engl. 40 (2001) 4570.
[92] U. Ryde, M.H.M. Olsson, B.O. Roos, A.C. Borin, Theor. Chem. Acc. 105 (2001) 452.
[93] P.M. Kozlowski, T.G. Spiro, A. Bérces, M.Z. Zgierski, J. Phys. Chem. Sect. B 102 (1998) 2603.
[94] A. Szabo, N.S. Ostlund, Introduction to Advanced Electronic Structure Theory, Dover, Mineola, 1982.
[95] C.J. Cramer, Essentials of Computational Chemistry, Wiley, Chichester, 2002.
[96] A. Veillard, in: G.H.F. Diercksen, B.T. Sutcliffe, A. Veillard (Eds.), Computational Techniques in Quantum Chemistry and Molecular Physics NATO ASI Series C, vol. 15, Reidel, Dordecht, 1975.
[97] H.B. Schlegel, J. Phys. Chem. 92 (1988) 3075.
[98] H.B. Schlegel, in: P.v.R. Schleyer, N.L. Allinger, T. Clark, J. Gasteiger, P.A. Kollman, H.F. Schaefer, III, P.R. Schreiner (Eds.), Encyclopedia of Computational Chemistry, Wiley, Chichester, 1998.
[99] G.D. Purvis, H. Sekino, R.J. Bartlett, Collect. Czech. Chem. Commun. 53 (1988) 2203.
[100] D.H. Magers, R.J. Harrison, R.J. Bartlett, J. Chem. Phys. 84 (1986) 3284.
[101] M.G. Cory, M.C. Zerner, J. Phys. Chem. Sect. A 103 (1999) 7287.
[102] M.G. Cory, Jr., K.K. Stavrev, M.C. Zerner, Int. J. Quant. Chem. 63 (1997) 781.
[103] D.H. Phillips, J.C. Schug, J. Chem. Phys. 61 (1974) 1031.
[104] A. Hardisson, J.E. Harriman, J. Chem. Phys. 46 (1967) 3639.
[105] K.M. Sando, J.E. Harriman, J. Chem. Phys. 47 (1967) 180.
[106] J.E. Harriman, J. Chem. Phys. 40 (1964) 2827.
[107] M.L. Munzarová, P. Kubáček, M. Kaupp, J. Am. Chem. Soc. 122 (2000) 11900.
[108] M. Munzarová, M. Kaupp, J. Phys. Chem. Sect. A 103 (1999) 9966.
[109] D. Feller, E.R. Davidson, in: K.B. Lipkowitz, D.B. Boyd (Eds.), Reviews in Computational Chemistry, vol. 1, VCH, New York, 1990.
[110] R. Krishnan, M.J. Frisch, J.A. Pople, J. Chem. Phys. 72 (1980) 4244.

[111] A.K. Wilson, T. van Mourik, T.H. Dunning, J. Mol. Struct. 388 (1996) 339.
[112] P.J. Hay, J. Chem. Phys. 66 (1977) 4377.
[113] W.J. Stevens, M. Krauss, H. Basch, P.G. Jasien, Can. J. Chem. 70 (1992) 612.
[114] G. Frenking, I. Antes, M. Böhme, S. Dapprich, A.W. Ehlers, V. Jonas, A. Neuhaus, M. Otto, R. Stegmann, A. Veldkamp, S.F. Vyboischchikov, in: K.B. Lipkowitz, D.B. Boyd (Eds.), Reviews in Computational Chemistry, vol. 8, VCH, New York, 1996.
[115] G. Barea, F. Maseras, A. Lledós, Int. J. Quant. Chem. 85 (2001) 100.
[116] K. Faegri, Jr., H.J. Speis, J. Chem. Phys. 86 (1987) 7035.
[117] W. Koch, M.C. Holthausen, A Chemist's Guide to Density Functional Theory, Wiley-VCH, Weinheim, 2000.
[118] L.J. Bartolotti, K. Flurchick, in: K.B. Lipkowitz, D.B. Boyd (Eds.), Reviews in Computational Chemistry, vol. 7, VCH, New York, 1996.
[119] R.G. Parr, W. Yang, Density-Functional Theory of Atoms and Molecules, Oxford University Press, Oxford, 1989.
[120] P. Hohenberg, W. Kohn, Phys. Rev. 136 (1964) B864.
[121] M. Levy, Proc. Natl. Acad. Sci. USA 76 (1979) 6062.
[122] W. Kohn, L.J. Sham, Phys. Rev. 140 (1965) A1133.
[123] D. Cremer, Mol. Phys. 99 (2001) 1899.
[124] R. Stowasser, R. Hoffmann, J. Am. Chem. Soc. 121 (1999) 3414.
[125] Q. Zhao, R.G. Parr, J. Chem. Phys. 98 (1993) 543.
[126] W. Yang, T.S. Lee, J. Chem. Phys. 103 (1995) 5674.
[127] V. Gogonea, L.M. Westerhoff, K.M. Merz, Jr., J. Chem. Phys. 113 (2000) 5604.
[128] G.D. Purvis, III, J. Comput.-Aided Mol. Des. 5 (1991) 55.
[129] P. Bouř, Chem. Phys. Lett. 345 (2001) 331.
[130] S.H. Vosko, L. Wilk, M. Nusair, Can. J. Phys. 58 (1980) 1200.
[131] T. Ziegler, Can. J. Chem. 73 (1995) 743.
[132] A.D. Becke, Phys. Rev. A 38 (1988) 3098.
[133] J.P. Perdew, Y. Wang, Phys. Rev. B 45 (1992) 13244.
[134] J.P. Perdew, Y. Wang, Phys. Rev. B 33 (1986) 8800.
[135] J.P. Perdew, Phys. Rev. B 33 (1986) 8822.
[136] C. Lee, W. Yang, R.G. Parr, Phys. Rev. B 37 (1988) 785.
[137] A.D. Becke, J. Chem. Phys. 98 (1993) 5648.
[138] P.J. Stephens, F.J. Devlin, C.F. Chabalowski, M.J. Frisch, J. Phys. Chem. 98 (1994) 11623.
[139] M.J. Frisch, G.W. Trucks, H.B. Schlegel, G.E. Scuseria, M.A. Robb, J.R. Cheeseman, V.G. Zakrzewski, J.A. Montgomery, R.E. Stratmann, J.C. Burant, S. Dapprich, J.M. Millam, A.D. Daniels, K.N. Kudin, M.C. Strain, O. Farkas, J. Tomasi, V. Barone, M. Cossi, R. Cammi, B. Mennucci, C. Pomelli, C. Adamo, S. Clifford, J. Ochterski, G.A. Petersson, P.Y. Ayala, Q. Cui, K. Morokuma, D.K. Malick, A.D. Rabuck, K. Raghavachari, J.B. Foresman, J. Cioslowski, J.V. Ortiz, B.B. Stefanov, G. Liu, A. Liashenko, P. Piskorz, I. Komaromi, R. Gomperts, R.L. Martin, D.J. Fox, T. Keith, M.A. Al-Laham, C.Y. Peng, A. Nanayakkara, C. Gonzalez, M. Challacombe, P.M.W. Gill, B.G. Johnson, W. Chen, M.W. Wong, J.L. Andres, M. Head-Gordon, E.S. Replogle, J.A. Pople, GAUSSIAN-98, Revision A.1., Pittsburgh, 1998.
[140] M. Von Armin, R. Ahlrichs, J. Comput. Chem. 19 (1998) 1746.
[141] T. Ziegler, A. Rauk, E.J. Baerends, Theor. Chim. Acta 43 (1977) 261.
[142] J. Gräfenstein, D. Cremer, Mol. Phys. 99 (2001) 981.
[143] J.A. Pople, P.M.W. Gill, N.C. Handy, Int. J. Quant. Chem. 56 (1995) 303.
[144] J. Baker, A. Scheiner, J. Andzelm, Chem. Phys. Lett. 216 (1993) 380.
[145] G.J. Laming, N.C. Handy, R.D. Amos, Mol. Phys. 80 (1993) 1121.
[146] C.J. Cramer, F.J. Dulles, D.J. Giesen, J. Almlöf, Chem. Phys. Lett. 245 (1995) 165.
[147] B.G. Johnson, C.A. Gonzales, P.M.W. Gill, J.A. Pople, Chem. Phys. Lett. 221 (1994) 100.
[148] J.M. Wittbrodt, H.B. Schlegel, J. Chem. Phys. 105 (1996) 6574.
[149] J. Wang, A.D. Becke, V.H. Smith, Jr., J. Chem. Phys. 102 (1995) 3477.
[150] M.-H. Whangbo, Theor. Chem. Acc. 103 (2000) 252.
[151] A. Ricca, C.W. Bauschlicher, Jr., J. Phys. Chem. 98 (1994) 12899.
[152] L. Andrews, G.V. Chertihin, A. Ricca, C.W. Bauschlicher, Jr., J. Am. Chem. Soc. 118 (1996) 467.
[153] M. Freindorf, P.M. Kozlowski, J. Phys. Chem. Sect. A 105 (2001) 7267.
[154] Y.-P. Liu, J. Chem. Inf. Comput. Sci. 41 (2001) 22.
[155] C. Rovira, K. Kunc, J. Hutter, P. Ballone, M. Parrinello, J. Phys. Chem. Sect. A 101 (1997) 8914.
[156] P.M. Kozlowski, T.G. Spiro, M.Z. Zgierski, J. Phys. Chem. Sect. B 104 (2000) 10659.
[157] D.A. Scherlis, C.B. Cymeryng, D.A. Estrin, Inorg. Chem. 39 (2000) 2352.
[158] D. Harris, G. Loew, L. Waskell, J. Inorg. Biochem. 83 (2001) 309.
[159] M.D. Segall, M.C. Payne, S.W. Ellis, G.T. Tucker, R.N. Boyes, Phys. Rev. E 57 (1998) 4618.
[160] D. Harris, G.H. Loew, A. Komornicki, J. Phys. Chem. Sect. A 101 (1997) 3959.
[161] M.R.A. Blomberg, P.E.M. Siegbahn, Theor. Chem. Acc. 97 (1997) 72.
[162] M.C. Zerner, in: K.B. Lipkowitz, D.B. Boyd (Eds.), Reviews in Computational Chemistry, vol. 2, VCH, New York, 1991.
[163] M.C. Zerner, G.H. Loew, R.F. Kirchner, U.T. Mueller-Westerhoff, J. Am. Chem. Soc. 102 (1980) 589.
[164] A.J. Boone, M.G. Cory, M.J. Scott, M.C. Zerner, N.G.J. Richards, Inorg. Chem. 40 (2001) 1837.
[165] F.H. Allen, S. Bellard, M.D. Brice, B.A. Cartwright, A. Doubleday, H. Higgs, T. Hummelink, B.G. Hummelink-Peters, O. Kennard, W.D.S. Motherwell, J.R. Rodgers, D.G. Watson, Acta Crystallogr. Sect. B 35 (1979) 2331.
[166] A.J. Boone, R.J. Bartlett, N.G.J. Richards, Inorg. Chem. (2002) submitted for publication.
[167] V.A. Rassolov, J.A. Pople, M.A. Ratner, T.L. Windus, J. Chem. Phys. 109 (1998) 1223.
[168] M.M. Francl, W.J. Pietro, W.J. Hehre, J.S. Binkley, M.S. Gordon, D.J. DeFrees, J.A. Pople, J. Chem. Phys. 77 (1982) 3654.
[169] P.C. Hariharan, J.A. Pople, Theor. Chim. Acta 28 (1973) 213.
[170] G.D. Fallon, B.M. Gatehouse, P.J. Marini, K.S. Murray, B.O. West, J. Chem. Soc. Dalton Trans. (1984) 2733.
[171] N. Govindaswamy, D.A. Quarless, Jr., S.A. Koch, J. Am. Chem. Soc. 117 (1995) 8468.
[172] M.R.A. Blomberg, P.E.M. Siegbahn, M. Svensson, J. Chem. Phys. 104 (1996) 9546.
[173] A. Ricca, C.W. Bauschlicher, Jr., J. Phys. Chem. Sect. A 101 (1997) 8949.
[174] B.N. Figgis, M.A. Hitchman, Ligand Field Theory and its Applications, Wiley-VCH, New York, 2000.
[175] C.J. Ballhausen, Introduction to Ligand Field Theory, McGraw-Hill, New York, 1962.
[176] M.I. Davis, A.M. Orville, F. Neese, J.M. Zaleski, J.D. Lipscomb, E.I. Solomon, J. Am. Chem. Soc. 124 (2002) 602.
[177] G.H. Loew, D.L. Harris, Chem. Rev. 100 (2000) 407.
[178] R.A. Edwards, M.M. Whittaker, J.W. Whittaker, E.N. Baker, G.B. Jameson, Biochemistry 40 (2001) 4622.
[179] A. Tanner, L. Bowater, S.A. Fairhurst, S. Bornemann, J. Biol. Chem. 276 (2001) 43627.
[180] J. Gao, in: K.B. Lipkowitz, D.B. Boyd (Eds.), Reviews in Computational Chemistry, vol. 7, VCH, New York, 1995.
[181] G. Monard, K.M. Merz, Jr., Acc. Chem. Res. 32 (1999) 904.

[182] J. Åqvist, A. Warshel, Chem. Rev. 93 (1993) 2523.
[183] P.A. Kollman, B. Kuhn, M. Peräkylä, J. Phys. Chem. Sect. B 106 (2002) 1537.
[184] M. Svensson, S. Humbel, R.D.J. Froese, T. Matsubara, S. Sieber, K. Morokuma, J. Phys. Chem. 100 (1996) 19357.
[185] A. Warshel, M. Levitt, J. Mol. Biol. 103 (1976) 227.
[186] W.D. Cornell, P. Cieplak, C.I. Bayly, I.R. Gould, K.M. Merz, Jr., D.M. Ferguson, D.C. Spellmeyer, T. Fox, J.W. Caldwell, P.A. Kollman, J. Am. Chem. Soc. 117 (1995) 5179.
[187] A.D. MacKerell, Jr., D. Bashford, M. Bellott, R.L. Dunbrack, Jr., J.D. Evanseck, M.J. Field, S. Fischer, J. Gao, H. Guo, S. Ha, D. Joseph-McCarthy, L. Kuchnir, K. Kuczera, F.T.K. Lau, C. Mattos, S. Michnick, T. Ngo, D.T. Nguyen, B. Prodhom, W.E. Reiher, III, B. Roux, M. Schlenkrich, J.C. Smith, R. Stote, J. Straub, M. Watanabe, J. Wiórkiewicz-Kuczera, D. Yin, M. Karplus, J. Phys. Chem. Sect. B 102 (1998) 3586.
[188] G.A. Kaminski, R.A. Friesner, J. Tirado-Rives, W.L. Jorgensen, J. Phys. Chem. Sect. B 105 (2001) 6474.
[189] W.L. Jorgensen, J. Tirado-Rives, J. Am. Chem. Soc. 110 (1988) 1657.
[190] D. Bakowies, W. Thiel, J. Phys. Chem. 100 (1996) 10580.
[191] J. Gao, P. Amara, C. Alhambra, M.J. Field, J. Phys. Chem. Sect. A 102 (1998) 4714.
[192] Y. Zhang, H. Liu, W. Yang, J. Chem. Phys. 112 (2000) 3483.
[193] M. Torrent, T. Vreven, D.G. Musaev, K. Morokuma, Ö. Farkas, H.B. Schlegel, J. Am. Chem. Soc. 124 (2002) 192.
[194] H. Liu, Y. Zhang, W. Yang, J. Am. Chem. Soc. 122 (2000) 6560.
[195] V. Guallar, B.F. Gherman, S.J. Lippard, R.A. Friesner, Curr. Opin. Chem. Biol. 6 (2002) 236.
[196] U. Rothlisberger, P. Carloni, K. Doclo, M. Parrinello, J. Biol. Inorg. Chem. 5 (2000) 236.
[197] C.J. Cramer, D.G. Truhlar, Chem. Rev. 99 (1999) 2161.
[198] V. Luzkhov, A. Warshel, J. Comput. Chem. 13 (1992) 199.
[199] M. Orozco, F.J. Luque, Chem. Rev. 100 (2000) 4187.
[200] S.N. Greene, A.J. Boone, W. Yang, N.G.J. Richards (2002) unpublished results.
[201] M.C. Colombo, L. Guidoni, A. Laio, A. Magistrato, P. Maurer, S. Piana, U. Röhrig, K. Spiegel, M. Sulpizi, J. VandeVondele, M. Zumstein, U. Röthlisberger, Chimia 56 (2002) 13.
[202] A. Magistrato, P.S. Pregosin, A. Albinati, U. Rothlisberger, Organometallics 20 (2001) 4178.
[203] C. Rovira, B. Schulze, M. Eichinger, J.D. Evanseck, M. Parrinello, Biophys. J. 81 (2001) 435.
[204] R.V. Pappu, R.K. Hart, J.W. Ponder, J. Phys. Chem. Sect. B 102 (1998) 9725.
[205] W.D. Cornell, P. Cieplak, C.I. Bayly, P.A. Kollman, J. Am. Chem. Soc. 115 (1993) 9620.
[206] C.M. Breneman, K.B. Wiberg, J. Comput. Chem. 11 (1990) 361.
[207] T.E. Cheatham, III, B.R. Brooks, Theor. Chem. Acc. 99 (1998) 279.